



## 1 **A review of analogue and numerical modelling in volcanology**

2 Janine L. Kavanagh<sup>\*1</sup>, Samantha Engwell<sup>2</sup> and Simon Martin<sup>1</sup>

3 <sup>1</sup>Department of Earth, Ocean and Ecological Sciences, University of Liverpool, Liverpool L69

4 3GP, United Kingdom

5 <sup>2</sup>British Geological Survey, The Lyell Centre, Research Avenue South, Edinburgh EH14 4AP,

6 United Kingdom

### 7 **Abstract**

8 Modelling has been used in the study of volcanic systems for more than one hundred years,  
9 building upon the approach first described by Sir James Hall in 1815. Informed by  
10 observations of volcanological phenomenon in nature, including eye-witness accounts of  
11 eruptions, geophysical or geodetic monitoring of active volcanoes and geological analysis of  
12 ancient deposits, analogue and numerical models have been used to describe and quantify  
13 volcanic and magmatic processes that span orders of magnitudes of time and space. We  
14 review the use of analogue and numerical modelling in volcanological research, focusing on  
15 sub-surface and eruptive processes including the accretion and evolution of magma  
16 chambers, the propagation of sheet intrusions, the development of volcanic flows (lava flows,  
17 pyroclastic density currents and lahars), volcanic plume formation and ash dispersal.

18 When first introduced into volcanology, analogue experiments and numerical simulations  
19 marked a transition in approach from broadly qualitative to increasingly quantitative  
20 research. These methods are now widely used in volcanology to describe the physical and  
21 chemical behaviours that govern volcanic and magmatic systems. Creating simplified  
22 depictions of highly dynamical systems enables volcanologists to simulate and potentially  
23 predict the nature and impact of future eruptions. These tools have provided significant  
24 insights into many aspects of the volcanic plumbing system and eruptive processes. The  
25 largest scientific advances in volcanology have come from a multidisciplinary approach,  
26 applying developments in diverse fields such as Engineering and Computer Science to study  
27 magmatic and volcanic phenomenon. A global effort in the integration of analogue and  
28 numerical volcano modelling is now required to tackle key problems in volcanology, and  
29 points towards the importance of benchmarking exercises and the need for protocols to be  
30 developed so that models are routinely tested against ‘real world’ data.

31 *Keywords: volcano, model, analogue model, numerical simulation*



32 **1.0 Introduction**

33 Volcanic activity is often unpredictable and occurs in an environment that is highly  
34 changeable and forbidding; however, there is a compelling need to improve our  
35 understanding of these complex systems. Approximately 800 million people around the world  
36 live close enough to a volcano to be directly affected by an eruption (Loughlin et al. 2015),  
37 and many more are at risk of social or economic impact as the consequences of volcanism  
38 extend from regional to potentially global areas (e.g. Svensen et al. 2004). The effects of an  
39 eruption can be felt long after an eruption has ceased, with the potential for both physical  
40 environments and societies to be impacted many decades after the event (e.g. the occurrence  
41 of lahars decades after the 1991 Mt. Pinatubo eruption, and the continuing impacts on  
42 communities following the Nevado del Ruiz eruption in 1985).

43 The challenges of working in volcanic terrains and gathering useful data mean that analogue  
44 and numerical models have gained significant importance in studying the dynamics of volcano  
45 growth and eruption. The occurrence of volcanic and magmatic activity is challenging and  
46 potentially impossible to forecast, and the factors that influence processes such as magma  
47 storage, ascent, eruption and deposition have several, often poorly constrained, variables.  
48 Technological limitations place boundaries on what we can record in nature; for example,  
49 direct observations are often problematic as the processes of interest are frequently hidden  
50 from view as they occur beneath the Earth's surface or within a pyroclastic flow or plume.  
51 The often remote and difficult to access location of volcanoes poses further logistical  
52 problems in studying processes.

53 Volcanic and magmatic processes occupy a vast range of scales from sub-millimetre to  
54 kilometres in size, and the timescales over which they take place range over fractions of a  
55 second up to millennia. The benefits of analogue and numerical modelling mean that it is  
56 possible to study these processes in a controlled environment, with the opportunity to repeat  
57 the phenomenon as required. Laboratory experiments and numerical simulations can link  
58 well-constrained starting conditions with measureable outcomes, and with careful scaling  
59 these findings can be extrapolated to better understand the natural processes. Quantitative,  
60 systematic and rigorous modelling in volcanology means "the contribution of experimental  
61 research to our understanding of volcanic processes is difficult to overstate" (Mader et al.  
62 2004).



63 In this invited review we will summarise the development of analogue and numerical  
64 modelling in the broad field of volcanology by providing some historical context and giving an  
65 overview of models that have been developed to study different parts of the system. Our  
66 intention is not to consider all parts of the magmatic and volcanic system, or review each area  
67 in depth, but instead to provide an account of the foundations of the subject, and to celebrate  
68 some of the key papers which have shaped modelling in volcanology. We describe some of  
69 the cutting-edge techniques that are being deployed to model volcanic and magmatic  
70 processes, considering magma and lava rheology, magma chambers, magma intrusions, lava  
71 lakes and lava domes, lava flows, pyroclastic density currents, lahars, volcanic plumes and ash  
72 dispersal (see Figure 1). We conclude by highlighting common challenges in the future of  
73 volcanology in our efforts to model these intriguing, captivating and potentially devastating  
74 phenomena.

## 75 **2.0 Historical context of modelling in volcanology**

76 Many of us have a profound fascination with volcanoes; from the beautiful landscapes they  
77 produce and art they inspire (see Sigurdsson (2015b) for a summary), to the impact their  
78 eruptions have on individuals, societies and civilizations (e.g. Sheets 2015). However, this  
79 fascination is often met with fear as the destruction volcanoes can cause may have far-  
80 reaching effects. The huge range of style and intensity of volcanic activity means that  
81 societies living nearby do so with high risk; there are however many benefits too, as volcanoes  
82 produce habitable environments on a local scale by the production of fertile soil and  
83 magmatic activity is associated with economic deposits such as copper porphyry. On a  
84 planetary scale the gases volcanoes emit lead to the creation of our oceans and the  
85 atmosphere. Life on Earth and the physical processes that govern volcanic activity are thus  
86 intimately connected.

### 87 **Volcanology as a science**

88 Our fear and fascination with volcanoes is evident in some of the earliest historical accounts  
89 of volcanic eruptions, which show that we have long tried to understand how volcanoes form  
90 and what causes them to erupt. Greek natural philosophers from the fifth and fourth century  
91 BC, such as Anaxagoras (c. 510-428 BC), Democritus (c. 460-370 BC) and Plato (c. 428-348 BC),  
92 proposed that volcanic eruptions were caused by ‘great winds inside the Earth’, an idea that



93 was supported by Aristotle (384-322 BC) (see Sigurdsson (2015a) for details). The study of  
94 volcanoes is founded on eye-witness accounts and field observations of activity, starting in  
95 Italy with the descriptions of Pliny the Younger of the eruption of Vesuvius in 79 AD. William  
96 Hamilton, a pioneer in volcanology, gained recognition for his descriptions of a much later  
97 eruption of Vesuvius in 1767 (Hamilton and Cadell, 1774). The interpretation of the origin of  
98 intrusive and extrusive igneous materials in the rock record came later with the seminal work  
99 of James Hutton (1726-1797), the so-called ‘Father of Geology’, whose field observations in  
100 1785 in the Cairngorm mountains, Scottish Highlands, demonstrated that granite rock was  
101 formed by the solidification of an initially liquid body that had intruded a pre-existing host  
102 rock (Hutton 1788).

### 103 **Experiments in volcanology and a quantitative approach**

104 Experimentation has long been an important tool in geological investigations. The first  
105 analogue experiments to study geological processes was published 200 years ago by James  
106 Hall in 1815. Hall’s experiments, carried out ‘with such materials as were at hand’, used  
107 several pieces of cloth, linen and wool each placed upon one another horizontally to  
108 represent a sequence of rock strata (see Figure 2). A rig then applied horizontal shortening  
109 to create a folded structure which Hall deemed reminiscent of convoluted rock layers at Fast  
110 Castle, Cockburnspath, Scotland. Hall’s research was read at a meeting of the Royal Society  
111 of Edinburgh, and has since inspired a new field of study using analogue materials to study  
112 geological processes in the laboratory. More specifically, the first experiments in volcanology  
113 used natural samples to explore the melting, crystallisation and fragmentation of igneous  
114 rocks. For example, Francesco d’Arezzo melted samples of lava from Etna in 1670 (Sigurdsson  
115 2015a), James Hall melted and then crystallised ‘whinstone’ (dolerite) and basaltic lavas in  
116 1790 (Hall 1805), and Auguste Daubrée performed volcanic diatreme analogue experiments  
117 to study vent processes and the formation of structures associated with diamondiferous  
118 kimberlite deposits (Daubrée 1891).

119 It wasn’t until the 1960’s that quantitative science started to emerge more prominently in the  
120 volcanological literature, transitioning away from largely qualitative and descriptive work. A  
121 pioneer in quantitative approaches in volcanology was George Walker (1926-2005), who is  
122 considered by many in the field to be the “the father of modern quantitative volcanology”  
123 due to his demonstration of how to integrate disciplines across the sciences, using field-based



124 measurements to develop and test conceptual models. The breadth of Walker's interests and  
125 expertise across volcanology were impressive, and his guidance and influence in the literature  
126 is evident across many parts of the volcanic system from plumbing systems, lava flows, tephra  
127 fall and flows (see Sparks (2009) for a review). Walker's quantitative approach, for example  
128 mapping the regional distribution of zeolites in Icelandic basalt lavas (Walker 1960) and being  
129 one of the first to publish calculations of lava flow viscosity based on field measurements of  
130 flow thickness, velocity and angle of slope (Walker 1967), led to the development of  
131 laboratory experiments in volcanology (and eventually numerical simulations) that could test  
132 hypotheses based on field data.

### 133 **Analogue and numerical modelling in volcanology**

134 The use of numerical and analogue modelling has come from the application of  
135 methodologies developed for alternative, sometimes quite disparate, purposes. From the  
136 1950's the fields of volcanology, fluid dynamics and engineering came together (Figure 3).  
137 Hubbert and Willis (1957) used gelatine solids injected with Plaster of Paris to study hydraulic  
138 fractures formed within pressurised boreholes, however the experiments also apply to  
139 modelling magma-filled fractures such as dykes and sills (Figure 3a); Fiske and Jackson (1972)  
140 subsequently used free-standing gelatine models to study magma propagation in a volcanic  
141 rift such as Hawaii (Figure 3b). The research of Morton et al. (1956) modelling industrial  
142 plumes rising from chimney stacks is the basis of many of the numerical models of volcanic  
143 plumes implemented today (Figure 3c). There are numerous examples where analytical  
144 models, numerical simulations and laboratory experiments have helped to explain processes  
145 that are too large or too complex to be understood in nature. George Walker and Lionel  
146 Wilson published experiments that studied the physics of pyroclastic fallout from large and  
147 highly explosive volcanic eruptions. They timed the fall of carefully characterized natural  
148 samples of tephra and compared these with theoretical computed terminal velocities to aid  
149 the analysis and interpretation of field deposits (Walker et al. 1971). Steve Sparks and Lionel  
150 Wilson developed early theoretical models to explore the controls of volcanic column height  
151 (Wilson et al. 1978) and the role of vent geometry on the collapse of eruptive columns to form  
152 ignimbrite deposits (Sparks & Wilson 1976). These works underpin much of the numerical  
153 and analogue modelling work conducted in volcanological research today.



### 154 **3.0 Parameterisation of models in volcanology**

155 Recent advancements in computational power, analytical techniques and experiment  
156 imaging have revolutionised numerical and analogue modelling in volcanology, ensuring their  
157 continued use in studying volcanic and magmatic phenomena. We define a numerical model  
158 as a set of algorithms and equations that are used to capture the physical or chemical  
159 behaviour of the system being modelled. We define an analogue model as a simplified  
160 representation of physical processes that is scaled down so it can be studied in the laboratory.  
161 Both analogue and numerical models are based on theoretical frameworks that have been  
162 developed to account for observations and measurements made in nature. Some of these  
163 models are directly informed by case studies, others are more generalised or focus on a  
164 specific process, and where possible the models are tested by comparing the model outputs  
165 with expected outcomes based on observed or measured phenomena. In engineering,  
166 analogue models are sometimes used to test and inform the development of numerical  
167 models; a numerical model of the analogue experiment is first created, and the results  
168 compared with those of the analogue experiment. This approach has great potential in  
169 volcanology, with examples in the field of tephra sedimentation and plume rise and  
170 formation, however the combination of analogue and numerical modelling is yet to be fully  
171 explored. By assessing the ‘mismatch’ between analogue and numerical models and testing  
172 the model outputs against natural observations, model errors can be quantified, incorrect  
173 assumptions investigated, and any limitations in the analogue or numerical model  
174 parameterisation can be identified (see Figure 4 for a flow diagram depicting model  
175 development and testing procedures).

176 Volcanic and magmatic processes are controlled by a range of physical processes and regimes,  
177 and these vary depending on whether subsurface or eruptive processes are being considered.  
178 For example, subsurface processes such as magma intrusion and conduit processes are largely  
179 controlled by the rheology of magma and deformation of the host rock, while eruptive  
180 processes are dependent on the density of an eruptive mixture and the characteristics of  
181 erupted products. Modelling volcanic mixtures is non-trivial due to their multiphase nature;  
182 magmas comprise melt, crystals and gas, while eruptive plumes and flows commonly  
183 comprise many different particle sizes, in addition to a gas phase. Fundamental to the  
184 success of models in volcanology is their parameterisation, with the model outputs strongly



185 dependent on the quality of the model inputs. However, there are different considerations  
186 that need to be made when developing a numerical model or analogue experiment.

### 187 **3.1 Numerical modelling**

188 Numerical modelling involves the selection and application of a number of mathematical,  
189 physical and/or chemical assumptions to represent a particular phenomenon. Modelling  
190 requires simplifications in the way a system is presented to be made. In deterministic  
191 modelling the model output is controlled by the model parameters and the initial conditions,  
192 whereas stochastic modelling involves an inherent randomness such that the same set of  
193 parameter values and initial conditions will produce a range of model outputs. In volcanology,  
194 the majority of numerical models are deterministic and the application of stochastic  
195 approaches is limited to hazard assessments.

196 Steady state models are used to estimate key parameters; however, they only give a first  
197 approximation of the physical behaviour and require assumptions to be made. For example,  
198 the thickness of a pyroclastic density current can be modelled at different distances from  
199 source, assuming eruption conditions such as source flux are constant through time. Transient  
200 models consider system changes over time, and are more complex and require the closure of  
201 more equations, but they are able to reproduce the unsteady behaviour observed in a range  
202 of volcanic phenomena.

203 Regardless of complexity, all numerical models require description of boundary conditions  
204 taking into account interaction with the surrounding environment. Examples of boundary  
205 conditions relevant to volcanic systems include atmospheric conditions when modelling  
206 eruption plumes, as humidity and wind strength exert a strong control over the height a  
207 volcanic plume may reach in the atmosphere, and stiffness of a host rock when modelling  
208 magma intrusions, as this will affect the propagation behaviour of a dyke or sill.  
209 Environmental conditions can be approximated in simplified numerical models, for example  
210 when modelling magma chamber growth the lithosphere may be modelled as a mechanically  
211 homogeneous material (e.g. Galgana et al. 2013) or by including mechanical heterogeneity  
212 and a stiffness contrast between crust and mantle (e.g. Le Corvec et al. 2015). Interactions  
213 between a phenomena and its surroundings are commonly accounted for in numerical  
214 models by simplified coefficients; for example the entrainment of ambient air into a rising



215 plume is described by two entrainment parameters: one considers radial entrainment due to  
216 turbulent eddies at the plume edge, and the other accounts for entrainment due to the  
217 effects of wind on the plume. These coefficients have been parameterised using a  
218 combination of both observations of the phenomena in nature and analogue experiments.

219 While it is possible to account for the effect of the ambient conditions on the modelled  
220 phenomena, it is considerably more difficult to account for feedback between the modelled  
221 phenomena and its environment as this requires significantly more computational power.  
222 Ultimately the results of any numerical simulation are dependent on the quality of input  
223 parameters, and these are either directly inferred from observations in nature or are  
224 estimated using analogue modelling (see Figure 4).

### 225 **3.2 Analogue modelling**

226 Analogue experiments are often three-dimensional models, although quasi-two-dimensional  
227 experiments are sometimes used. Parameterisation of analogue models requires the  
228 development of appropriate scaling laws and then careful material characterisation at  
229 experimental conditions. The choice of analogue material will depend on the parameters that  
230 are being investigated and the conceptual model that is being tested; many simplifications  
231 are required in order to track the impact of variables on experiment outcomes, e.g. how  
232 changes in density contrast between fluid and surroundings effect geometry, velocity or  
233 pressure. Extracting and measuring parameters and variables in analogue experiments is  
234 crucial for understanding the modelled phenomena, and for checking model  
235 parameterisation is consistent with appropriate scaling laws.

#### 236 ***3.2.1 Scaling experiments and choosing analogue materials***

237 The principles and methods to scale laboratory experiments were laid down by M. King  
238 Hubbert (1937) in a seminal paper that sets out the foundation upon which all analogue  
239 modelling should be undertaken. He stated that the choice and characterisation of analogue  
240 materials need to be carefully considered in reference to geometric, kinematic and dynamic  
241 scaling laws between the laboratory and natural components in order for experimental  
242 results to be applied back to nature. In the study of subsurface processes in volcanology, such  
243 as magma intrusion, scaling laws mean that it is possible to create a scaled laboratory  
244 experiment where several of the scaling criteria, e.g. based on model ratios that take into



245 account length, time and forces, can be met by using a selection of domestic fluids, powders  
246 and gels. An early advocate of Hubbert's approach was Ramberg (1967) who used these  
247 principles to develop centrifugal models using silicone putty to model diapirs. Scaled  
248 analogue experimentation has since been applied in a huge range of geological contexts,  
249 using model ratios for magma and rock or using the pi theorem (e.g. Merle, 2015). Although  
250 compromises are nearly always needed, there are particular challenges for using analogue  
251 experiments to study conduit and eruptive processes. Recent review papers on scaling  
252 laboratory experiments in volcanology include Galland et al. (2015) and Merle (2015).

253 Once scaling laws have been determined, appropriate analogue materials need to be  
254 selected. To assist with this, temperature-dependant Newtonian and non-Newtonian fluids  
255 and gels have been characterised in a viscometer or rheometer at a controlled temperature  
256 and using a range of measurement geometries; these include rotary, concentric cylinder,  
257 falling ball, tube and parallel plate methods. A known shear stress ( $\sigma$ ) is applied to a small  
258 sample of the fluid or gel, and the strain ( $\gamma$ ) or strain rate ( $\dot{\gamma}$ ) required to meet this stress is  
259 measured. The material's viscosity ( $\eta$ ) is thus characterised, and the material properties can  
260 often be tailored so that it meets the required physical behaviour which can be used to help  
261 relate the experiment results back to nature.

### 262 ***3.2.2 Experiment imaging techniques***

263 There have been several recent developments in imaging and measuring experiment  
264 parameters and variables in the laboratory, drawing on technologies developed for industrial  
265 purposes to study volcanic processes. For a complete description, imaging and  
266 measurements need to focus on detailed external and internal monitoring of an analogue  
267 experiment.

268 Photogrammetry enables measurements to be made from photographs with great precision  
269 and can be used to construct three-dimensional representations of real-world objects. The  
270 open-source photogrammetric software MicMac (e.g. Galland et al. 2016) uses Structure-  
271 from-Motion algorithms to process experiment images from synchronised cameras and for  
272 example create a time-series of digital elevation models (DEMs) representing the changes in  
273 the surface of an experiment. X-ray micro-tomography can produce high resolution three-  
274 dimensional reconstructions of a static model topography with cross-sections showing



275 internal structures; though the imaging is limited to small experiments, variation in signal to  
276 noise ratio and the need to have stable models during the duration of the scan (e.g. Kervyn  
277 et al. 2010). Dynamic processes can be studied for example using gelatine as a host-rock  
278 material which enables stress to be imaged when it is deformed and then viewed with  
279 polarised light. An interference pattern and colour fringes are produced due to gelatine's  
280 photoelastic properties (Crisp 1952). This method allows differential stresses and their  
281 evolution to be mapped qualitatively during an experiment (see Section 6 for examples).  
282 Lasers can also be used to illuminate a thin vertical sheet within a gelatine experiment (e.g.  
283 Kavanagh et al. 2015, 2017) or particle suspension experiment (e.g. Andrews and Manga  
284 2012), with images recorded at time-defined intervals. Techniques such as Digital Image  
285 Correlation (DIC) can then be used to map internal strain changes for example within gelatine  
286 with suspended fluoresced tracer particles. Particle Image Velocimetry (PIV), which is a  
287 comparative technique to DIC, can be used to map fluid flow and produces instantaneous  
288 velocity measurements using passive-tracer seeding particles within the fluid, e.g. water as  
289 an analogue for magma within a dyke (e.g. Kavanagh and Dennis 2014, 2015) and particulate  
290 suspension in a pyroclastic density current or volcanic plume (Andrews and Manga 2012).  
291 The ability to integrate measurements of the surface and subsurface development of, for  
292 example, magma intrusion in the laboratory greatly strengthens the ability of analogue  
293 experimentation to help inform numerical modelling that is used to interpret volcano-  
294 deformation data in nature.

295 In the following sections, we describe and discuss the range of analogue and numerical  
296 modelling methods and techniques that have been applied to different physical volcanic  
297 processes.

#### 298 **4.0 Magma and Lava Rheology**

299 Magma is one of the principal components of a volcanic system and the modelling of magma  
300 encompasses the study of magma chambers, volcanic plumbing systems, conduit processes,  
301 the development of lava domes and flows, and magma fragmentation in explosive eruptions.  
302 It is for this reason that a review of modelling in volcanology must start with models of magma  
303 and lava rheology. Numerical models of magma have focused on the development of  
304 analytical solutions that can account for the range of conditions that magma is subjected to



305 from source to surface. Analogue experiments have aided the development of these  
306 numerical models using scaled analogue materials which test and help to build a theoretical  
307 framework for modelling magma.

308 Magma can be modelled as a multi-phase fluid, comprising a melt phase with variable  
309 proportions of bubbles and crystals. Single-phase magmas (melt only) are very rare, and  
310 possibly only occur deep within the crust. Silicate melts are often modelled as a Newtonian  
311 fluid with constant viscosity (Lejeune & Richet 1995; Ishibashi 2009):

$$312 \quad \eta = \frac{\sigma}{\dot{\gamma}} \quad [1]$$

313 where viscosity ( $\eta$ ) is the ratio of shear stress ( $\sigma$ ) and strain rate ( $\dot{\gamma}$ ). Several types of non-  
314 Newtonian rheology have been applied to model the behaviour of magmas and lavas based  
315 on field observations. A Bingham fluid has to overcome a yield stress before it can begin to  
316 flow (Hulme 1974):

$$317 \quad \eta = \frac{\sigma - \sigma_0}{\dot{\gamma}} \quad [2]$$

318 where  $\sigma_0$  is the initial shear stress required to cause the onset of flow when  $\dot{\gamma} = 0$ . Once the  
319 yield stress has been overcome, the fluid has a constant viscosity. More recently, the Herschel  
320 Bulkley model (Herschel & Bulkley 1926) has been applied to the behaviour of magmas  
321 (Llewellyn, Mader & S. Wilson 2002b; Mueller et al. 2011) due to its versatility in allowing for  
322 the modelling of a spectrum of magma behaviours (Newtonian, shear thinning, shear  
323 thickening):

$$324 \quad \sigma = \sigma_0 + K\dot{\gamma}^n \quad [3]$$

325 where  $\sigma_0$  is yield stress when there is no flow,  $K$  is the consistency ( $\eta$  when  $\dot{\gamma} = 1$ ), and  $n$  is the  
326 degree of non-Newtonian behaviour (where  $n = 1$  is Newtonian,  $n < 1$  is shear-thinning, and  
327  $n > 1$  is shear-thickening).

#### 328 **4.1 Two-phase suspensions: Particle suspensions**

329 Modelling the behaviour of particulate suspensions is crucial for describing the physical  
330 behaviour of volcanic processes. Particulate suspensions are ubiquitous across a volcanic  
331 system, from crystals in magma to ash particles within an eruptive plume. Within magmas,  
332 variations in crystal content mostly originate from changes in temperature, but the particle



333 size within a volcanic plume or pyroclastic density current is related to the type of eruption  
 334 (phreatomagmatic eruptions have significantly smaller particle sizes than magmatic eruptions  
 335 for example). For the purposes of numerical and analogue modelling, particle distributions  
 336 are simplified with either a single well-defined particle size or a small number of particles sizes  
 337 used to replicate natural systems (e.g. Figure 5a-c). However, both numerical and analogue  
 338 studies have shown that particulate concentration has a first order control on eruptive  
 339 behaviour. In volcanic plumes, higher particulate concentrations, relating to higher plume  
 340 densities, lead to column collapse, as shown by the analogue experiments of Carey et al.  
 341 (1988). In addition, numerical studies have shown that particle concentration has a first order  
 342 control on initiation of coignimbrite plumes (Engwell et al. 2016).

#### 343 4.2 Two-phase suspensions: Bubble suspensions

344 The effect that bubbles have on magma viscosity depends on bubble shape, size and ability  
 345 to deform under stress. In steady flow regimes, where stress and shear are constant, the  
 346 bubbles reach an equilibrium deformation defined by the capillary number  $Ca$  (Manga &  
 347 Loewenberg 2001; Llewellyn et al. 2002b):

$$348 \quad Ca = \frac{\eta_0 r \dot{\gamma}}{\Gamma} \quad [4]$$

349 where  $\eta_0$  is the fluid viscosity without bubbles,  $r$  is the un-deformed bubble radius,  $\dot{\gamma}$  is strain  
 350 rate, and  $\Gamma$  is interface surface tension between the liquid and gas. Small capillary numbers  
 351 are dominated by surface tension, meaning that bubbles reach their equilibrium deformation  
 352 soon after there is a change in shear rate (Llewellyn et al. 2002a; Llewellyn et al. 2002b), and  
 353 they produce spherical bubbles that act to increase the viscosity of the suspension by creating  
 354 an obstacle to flow. Large capillary numbers give rise to easily deformable and often elongate  
 355 bubbles, acting as sites where shear localization can occur due to a reduction in friction, and  
 356 will reduce bulk viscosity (Manga et al. 1998; Mader et al. 2013).

357 In unsteady flow regimes, when there is a variable strain rate, the forces causing deformation  
 358 and restoration of the bubble shape are not in equilibrium (Llewellyn et al. 2002b). As such  $Ca$   
 359 number (equation 4) does not adequately describe the behaviour of the bubble, and so a  
 360 dynamic capillary number  $Cd$  is defined:

$$361 \quad Cd = \lambda \frac{\ddot{\gamma}}{\dot{\gamma}} \quad [5]$$



362 where  $\dot{\gamma}$  is the rate of change of the imposed deforming force. This relationship explains how  
363 bubbles behave under time-dependant shear conditions.

#### 364 4.3 Three-phase suspensions

365 Three-phase suspensions are well suited to explaining the behaviour of magmas and bring us  
366 closer to understanding the volcanic systems, but they also present several challenges  
367 associated with the additional complexity modelled.

368 A three-phase suspension can be modelled assuming a bubble suspension base fluid with the  
369 particles suspended within (Truby et al. 2015; see Figure 5d):

$$370 \frac{\eta^*}{\eta_b} = \left(1 - \frac{\varphi_p}{\varphi_m}\right) \quad [6]$$

371 where  $\eta^*$  is relative viscosity,  $\eta_b$  is bubble suspension viscosity,  $\varphi_p$  is particle volume fraction  
372 and  $\varphi_m$  is the maximum packing fraction. This simplifies the calculation of the three-phase  
373 rheology, and assumes a low bubble capillarity (see Truby et al. 2015, eq. 3.2); however if this  
374 is not appropriate then the bubble viscosity  $\eta_b$  may need to be substituted by a high bubble  
375 capillarity viscosity equation. This new model can account for a crystal bearing magma that  
376 has no bubble content at depth but vesiculates during ascent. It therefore marks a significant  
377 advancement in our understanding of magma behaviour through time and space, and will be  
378 an important tool in future models to better constrain the impact of three-phase magma  
379 rheology on volcanic eruptions. Gas escape and the development of permeable pathways in  
380 particle-rich suspensions has applications to the study of degassing crystal-rich magmas, with  
381 analogue experiments showing that migration patterns (either by bubble formation or  
382 fracture-like) are controlled by particle fraction and the degree of particle-packing (see Figure  
383 5e; Oppenheimer et al. 2015).

384 Depending on the application and level of complexity, a variety of analogue materials have  
385 been used to model magma (see Table 1 for a summary). Many models use a melt-only  
386 magma analogue for simplicity, or in more complex models two-phase suspensions (bubbles  
387 in liquid, or crystals in liquid) and rarely three-phase (bubbles and crystals in a liquid). As  
388 such, the spectrum of rheology that has been considered in magma analogue models is broad  
389 and includes the use of Newtonian fluids, Bingham fluids or Herschel-Bulkley.



## 390 **5.0 Magma Chambers**

391 Magma chambers are the deepest and therefore arguably the most obscure parts of the  
392 volcanic and magmatic system. The relationship between large, ancient magma bodies, such  
393 as laccoliths and plutons, and magma chambers that feed volcanic eruptions is enigmatic and  
394 currently under debate (e.g. Lundstrom & Glazner 2016). Plutons are large accumulations of  
395 coarse-grained igneous rock and they express a broad range of compositions, generally falling  
396 between granite and gabbro, with physical properties (such as viscosity) that can span several  
397 orders of magnitude and vary both in space and time. A growing body of literature challenges  
398 the traditional “big tank” conceptual model of magma chambers as dynamic, large and long-  
399 lived accumulation of magma that slowly cools, crystallises and differentiates (Glazner et al.  
400 2004). Instead it is proposed that large igneous bodies and magma chambers are  
401 incrementally emplaced from the accumulation of sill-like bodies (horizontal planar magma-  
402 filled sheets), and that they are discrete and ephemeral regions of melt and mush (Figure 1;  
403 see Annen et al. 2015 for a review).

### 404 **5.1 Analogue models of magma chambers**

#### 405 **High viscosity magmas**

406 Examples where large magma bodies have been studied experimentally in the laboratory are  
407 relatively rare. Pluton emplacement has been modelled as a large body of viscous fluid which  
408 plastically deforms its surroundings, focusing on pluton geometry and how space is  
409 accommodated in the lithosphere. Perhaps one of the earliest analogue experiments to study  
410 granitic pluton emplacement was by Ramberg (1970) who used a combination of clay, putties,  
411 wax-oil mixtures, plates of concrete and aqueous solutions to simulate diapiric ascent of fluid-  
412 like magmas through rock layers with differing competency (see Tables 1 and 2). In his  
413 experiments, Ramberg used a centrifuge model arrangement capable of reaching an  
414 acceleration of 4000 x g to assist with scaling. Roman-Berdiel et al. (1997) and Roman-Berdiel  
415 (1999) studied granite emplacement by injecting low-viscosity Newtonian silicone putty into  
416 a tank of sand. Processes such as granite intrusion under the influence of tectonic stresses  
417 (Mazzarini et al. 2010), interaction with coincident faults and fractures during transpression  
418 (Benn et al. 1998) and strike-slip (Corti et al. 2005) motion have also been considered.

#### 419 **Low viscosity magmas**



420 Several papers were published in the 1980's exploring the cooling of a large predominately-  
421 liquid magma reservoir using analogue models, studying the so-called 'double diffusive  
422 convection' model and its application to magma chamber evolution (Huppert & Turner  
423 1981b). The double diffusive convection model accounts for convection of a fluid with  
424 composition and temperature gradients acting in opposing directions. It was originally  
425 derived from oceanographic applications, yet has proved helpful to explain geological  
426 features such as large-scale cyclic crystal layering within large igneous bodies and supports  
427 the proposed conceptual model that magma chambers are compositionally zoned (Huppert  
428 & Sparks 1980). Subsequent analogue models have investigated magma mixing and magma  
429 mingling, for example for the case of a rhyolite magma chamber injected by basalt from below  
430 (Huppert et al. 1983) or mafic magma chambers replenished by felsic injections (Weinberg  
431 and Leitch 1998). The impact of volatile exsolution and bubble formation on magma mixing  
432 was explored in the laboratory by Huppert et al. (1982) and Turner et al. (1983) by introducing  
433 reactive  $\text{HNO}_3$  into liquid layers of  $\text{K}_2\text{CO}_3$  (upper layer) and  $\text{KNO}_3$  (lower layer) to cause the  
434 release of gas. Phillips and Woods (2001) then studied the accumulation of bubbles and  
435 movement of bubbles within a magma chamber, using a salt solution as the magma analogue  
436 and an electrolysis cell with gauze to produce the bubbles. All these studies demonstrated  
437 that a recharge event of bubble-rich and low density magma, such as basalt, into a magma  
438 chamber may generate a turbulent bubble plume within the chamber that can be described  
439 by plume theory. Such bubble plumes could impact magma mixing within the chamber, the  
440 stability of the magma chamber, have the potential to trigger an eruption and could affect  
441 the style of eruptive activity. Magma contamination from roof and wall melting has also been  
442 studied experimentally (Leitch 2004).

#### 443 **Magma chamber failure**

444 Fracture and failure of a magma chamber to feed a volcanic eruption has also been studied  
445 in analogue experiments, studying the nucleation of magma-filled fractures (dykes). McLeod  
446 and Tait (1999) used gelatine models to study the pressurisation and failure of liquid-filled  
447 cavities, creating a crustal 'magma chamber' by inflating a balloon within the liquid gelatine  
448 and removing it when the gel had solidified. Fluid was then injected into the cavity using a  
449 head pressure. Under increasing stress and strain, the gelatine undergoes an initially elastic  
450 deformation and then brittle failure. They found that dyke nucleation occurred from a pre-



451 existing flaw in the analogue chamber wall, and that the viscosity of the fluid influenced the  
452 tendency for dykes to propagate. Koyaguchi and Takada (1994) also used gelatine models and  
453 glycerine to explore how the evacuation of a low viscosity fluid may lubricate the path of a  
454 more viscous fluid into a pre-existing fracture. Earthquakes are also potentially an important  
455 external influence on magma chamber stability that may trigger dyking that leads to a volcanic  
456 eruption. Namiki et al. (2016) considered two different scenarios of foam stability over a liquid  
457 layer of diluted glucose syrup in a partially filled tank (open vent) or fully-filled tank with  
458 density-stratified fluids (sealed magma reservoir). The use of a shaking table enabled the  
459 authors to identify the conditions for 'sloshing' of the magma chamber to occur. They found  
460 that the foam layer completely collapsed when oscillations were near the resonance  
461 frequency of the fluid layer and when sloshing low viscosity fluids surrounding large bubbles.  
462 In nature the collapse of a foam would potentially release a gas slug and produce a magmatic  
463 eruption, or result in magma overturn and a delayed eruption.

## 464 **5.2 Numerical models of magma chambers**

465 Increasingly complex Finite Element Modelling (FEM) techniques are being developed to  
466 account for the evolving thermo-mechanical and chemical processes associated with magma  
467 chamber recharge events. Such techniques are applied to volcanic centres that are  
468 experiencing periods of unrest to infer characteristics of the magma chamber including depth,  
469 overpressure, volume change and shape (e.g. Hickey et al. 2016; see Figure 6a). However  
470 numerical modelling of magma accumulation in the crust is generally one-dimensional.

471 Annen et al. published a series of papers that accounts for the generation of intermediate and  
472 silicic magmas in Deep Hot Zones based on a heat-transfer numerical model that simulates  
473 magma injection in the crust or crust-mantle boundary and calculates the conditions required  
474 for the accumulation of melt to build a reservoir of eruptible magma (e.g. Annen et al. 2006a;  
475 Annen et al. 2006b; Annen 2009). The equilibrium thermodynamic model is based on a heat  
476 balance between injected magma and surrounding rock; parameters such as density, specific  
477 heat capacity, temperature, time, melt fraction, latent heat of fusion, thermal conductivity  
478 and depth are included. These models have calculated that a 10 km thick pluton requires a  
479 magma flux that exceeds  $10^{-2} \text{ km}^3/\text{yr}$  to permit the development of a magma chamber with a  
480 volume of eruptible magma sufficient to feed the largest silicic explosive eruptions (Annen  
481 2009).



482 The occurrence of plutons that are layered mafic intrusions (LMI's) has been invoked as a  
483 record of dynamic processes that can occur within magma chambers. Bons et al. (2014)  
484 developed a simple finite difference one-dimensional model that simulates the vertical profile  
485 of evolving crystal fraction of an initially liquid magma chamber. Similarly to 'traffic jam'  
486 theory, their models suggest that self-organization of crystals will occur in a cooling magma  
487 reservoir due to gravitational sorting of floating or settling crystals. The distance the crystals  
488 travel depends on parameters such as melt viscosity and cooling rate; as the crystals interact  
489 barriers may form which instigate layers to develop, each of which then undergoes similar  
490 crystal sorting. This could explain rhythmic layering but also larger scale zonation observed  
491 in large igneous bodies.

### 492 **5.3 Testing magma chamber models**

493 The numerical simulations and analogue models of magma chamber dynamics can be tested  
494 against modern case studies with recent volcanic activity (e.g. the Soufriere Hills volcano,  
495 Montserrat (Annen et al. 2014; see Figure 6b)) but also against the rock record to help  
496 interpret whether an exposed pluton was once a magma chamber or several discrete and  
497 small magma bodies (e.g. the Torres del Paine Intrusive Complex, Chile (Leuthold et al. 2012),  
498 and the Tuolumne Intrusive Suite, Sierra Nevada, USA (Coleman et al. 2004)). One current  
499 limitation of numerical models of magma chambers is that they are static and for example do  
500 not consider magma injection mechanisms. There is therefore scope for more interaction  
501 between numerical and analogue modellers of magma chambers, with great potential to  
502 advance our understanding of this dynamic and yet highly enigmatic component of volcanic  
503 systems.

### 504 **6.0 Magma Intrusions**

505 Magma transport through the crust is facilitated by a series of interconnected magma-filled  
506 sheet intrusions called dykes and sills (see Figure 1). Together these comprise a volcanic  
507 plumbing system that stores magma at depth but also can directly feed eruptions at the  
508 surface. A key assumption in many models is that sills are fed by dykes. The modelling  
509 approach depend on the assumptions on the controls of magma intrusion: 1) magma  
510 intrusion is modelled as a hydraulic fracture using the principles of linear elastic fracture  
511 mechanics (LEFM) and propagation is driven by fracturing of the host rock, or 2) magma



512 intrudes as a viscous indenter and the growth dynamics are governed by the plastic  
513 deformation of the host and fluid properties of the magma.

#### 514 **6.1 Analogue models of sheet intrusion**

515 To study the intrusion of magma-filled fractures in the laboratory, scaling of both magma and  
516 host-rock materials and their interaction needs to be considered. Two types of host-rock  
517 analogues are commonly used depending on the model being explored: gels such as gelatine  
518 for modelling intrusions as hydraulic fractures, and granular materials such as compacted  
519 silica flour to model them as viscous indenters. Magma analogues include air, water or a  
520 solidifying fluid such as vegetable oil (most frequently Vegeteline). Tables 1 and 2 describe  
521 material properties of magma and host-rock analogue materials and the combinations they  
522 have been used to study sheet intrusions.

##### 523 ***6.1.1 Gelatine models of hydraulic fractures***

524 Gelatine has been used as an analogue host material for magmatic sheet intrusions since  
525 Hubbert and Willis (1957) injected a plaster-of-Paris slurry ‘fracturing fluid’ into a gelatine  
526 solid to study hydraulic fractures (Figure 3a). For decades since, this material has been used  
527 to investigate the dynamics of magma intrusions considering a large range of parameters such  
528 as density contrasts between magma and host rock, impact of a stress field and mechanical  
529 layering of host rocks.

530 Gelatine mixtures are slightly denser than water (see Table 1), and the magma analogue that  
531 is used (e.g. air or water) is often buoyant and injected into the gelatine slab using a pump  
532 which supplies the fluid at a controlled flux or pressure. The dyke which is created takes the  
533 form of a penny-shaped crack, as expected by theoretical models of a pressurised fluid-filled  
534 crack in an elastic medium, but can become isolated from its injector (Takada 1990); in doing  
535 so its geometry changes from elliptical to teardrop with a rounded head and pinched lower  
536 tip (e.g. Weertman 1971, see Figure 7a for an example). Menand and Tait (2001) showed how  
537 liquid and gas mixtures injected into gelatine become segregated, with gas moving into the  
538 dyke tip region and liquid into the tail region. The buoyant gas then had a dominant control  
539 on the propagation dynamics of the dyke.

#### 540 **Impact of mechanical layering of the crust on magma intrusion**



541 Mechanical heterogeneities such as layering and the presence of discontinuities has been  
542 shown to influence the propagation of a fluid-filled crack in an elastic gelatine host material.  
543 Le Corvec et al. (2013) studied magma ascent in fractured crustal rocks by injecting air into a  
544 gelatine slab that has been pre-cut in its upper part to mimic the presence of faults and  
545 fractures in the lithosphere. They found that dyke geometry and dynamics were affected by  
546 the presence of the fractures, and a dyke would decelerate as it began to propagate between  
547 two fractures. A layered crustal analogue can be created by varying gelatine concentration  
548 (e.g. Kavanagh et al. 2013), and the strength of the bonded interface between layers is  
549 controlled by the temperature contrast between layers during experiment preparation  
550 (Kavanagh et al. 2015; 2017). The conversion from a dyke to a sill in gelatine experiments  
551 (e.g. Rivalta et al. 2005; Kavanagh et al. 2006) depends on the rigidity contrast between the  
552 layers and the fracture toughness (ability to resist fracture) of their bonded interface, with a  
553 rigid upper layer and weak interface being most favourable for the dyke-to-sill transition and  
554 dyke-sill hybrid structures formed in intermediate regimes (Kavanagh et al. 2017). Layered  
555 gelatine experiments have also been used to study laccolith emplacement whereby viscous  
556 grease was injected into layered-gelatine with a lubricated interface (Pollard 1973; Pollard &  
557 Johnson 1973; Johnson & Pollard 1973).

#### 558 **Interaction of magma-filled fractures with a stress field**

559 The orientation of dykes in nature suggests they can be strongly influenced by the stress field  
560 in which they propagate, and this process has been explored in gelatine analogue  
561 experiments. Fiske and Jackson (1972) used a gelatine solid to study the impact of  
562 gravitational forces on the trajectory of magma injections in the crust applied to volcanic rifts  
563 in Hawaii (Figure 3b). They used a variety of moulded shapes of gelatine such as linear, ridge-  
564 shaped and curved-tapered ridge-shaped which visibly deformed due to gravity when  
565 released from their mould and adhered to a surface. When injected with dyed water the  
566 dykes moved laterally following the ridge axis (straight or curved). The experimental dykes  
567 were vertical, oriented perpendicular to the least compressive stress direction and  
568 propagated in the direction of the ridge. Subsequent gelatine studies have investigated dyke  
569 injection into a conical edifice (e.g. McGuire & Pullen 1989) and have explored the impact of  
570 the formation of a collapse scarp on dyke orientation (e.g. Walter & Troll 2003).



571 Dyke injection into gelatine under extension was studied by Daniels and Menand (2015) as an  
572 analogue for magma propagation in the Afar rift zone; extension was created by applying a  
573 uniform load to the entire surface of the gelatine and therefore compressing it from above  
574 with the gelatine slab margins moved outwards to occupy a water-filled margin. They found  
575 that the orientation of an experimental dyke in this environment was perpendicular to the  
576 maximum extensional stress, and that the dyke arrested beneath a thin rigid layer.  
577 Subsequent dyke orientations were affected by the ratio of the overpressure of the  
578 unerupted initial injection and the remote tensile stress, causing a rotation to occur. Menand  
579 et al. (2010) investigated the impact of stress reorientation on the propagation path of  
580 buoyant magma-filled fractures using air injected into gelatine. To create a lateral deviatoric  
581 compressive stress field in the initially hydrostatic slab, they inserted vertical plates between  
582 the solidified gelatine and tank walls exerting uniform compression across the whole slab such  
583 that  $\sigma_1$  was horizontal and  $\sigma_3$  was vertical. Their results showed that a buoyant, initially  
584 vertical dyke rotated to propagate horizontally and form a sill in response to the imposed  
585 stress field and following the direction of the maximum compressive stress  $\sigma_1$ . The impact of  
586 the load from a volcanic edifice on dyke propagation, dyke trajectory and eruption has also  
587 been studied using gelatine experiments (e.g. Hyndman and Alt 1987; Muller et al. 2001;  
588 Kervyn et al. 2009; see Figure 7b). When dyke injection was offset from the centre of the  
589 edifice it acted as an attractor to the dyke, causing the initially vertical trajectory to be  
590 deflected towards the load. Dyke ascent from directly beneath the edifice was initially vertical  
591 and then either stalled or changed to propagate laterally and caused a ‘flank’ eruption at the  
592 cone base (see Figure 7b).

593 Due to the photoelastic properties of gelatine, stress in the host material associated with the  
594 formation and growth of fluid-filled dykes and sills is shown in polarised light (e.g. Kavanagh  
595 et al. 2017; see Figure 7a and 8a). The evolution of incremental and finite strain in the  
596 deforming gelatine due to dyke, sill and hybrid intrusions has been quantified using DIC using  
597 passive-tracer particles suspended within the gelatine layers illuminated by a thin, vertical  
598 laser sheet (Kavanagh et al. 2015; 2017; see Figure 8b). This analysis has shown there are  
599 significant (up to 60%) decreases in strain around a feeder dyke as a sill forms (Kavanagh et  
600 al. 2015; 2017; see Figure 8c). As gelatine deformed elastically at the experimental conditions  
601 (e.g. Kavanagh et al. 2013; Van Otterloo and Cruden 2016), the decrease in strain correlates



602 with a decrease in stress. At the feeder dyke margin this stress change can be directly linked  
603 to a decrease in fluid pressure when the sill forms (Kavanagh et al. 2015; 2017).

#### 604 ***6.1.2 Compacted granular materials and viscous indenters***

605 Compacted fine-grained silica flour has been used as a host-rock analogue where magma  
606 intrusion is modelled as a viscous indenter. This material can fail both in tension and in shear  
607 due to its non-negligible cohesion. Other comparable granular materials that have been used  
608 to study sheet intrusions include ignimbrite, diatomite and dry plaster powder which, in  
609 general, are fine grained frictional, cohesive and variably permeable (see Table 1 for material  
610 properties and Table 2 for host-rock and magma analogue combinations). Factors such as the  
611 surface deformation associated with sheet intrusion and the impact of mechanical layering  
612 and ambient stress field have been considered using these materials. As they are opaque this  
613 requires solidifying fluids to be injected (often Vegetaline, see Table 2) and then either the  
614 resulting intrusion is excavated post-emplacment and its dimensions linked to surface  
615 deformation (see Figure 8d for an example experiment setup), or a thin quasi-two-  
616 dimensional tank is used to show a cross-section through the experiment as intrusions form.  
617 A variety of analogue intrusions have been created in compacted silica flour experiments,  
618 ranging from cone sheets to dykes and sills (Galland et al. 2014; see Figure 7c). Galland et al.  
619 (2016) used the photogrammetry software MicMac to reconstruct their three-dimensional  
620 excavated solidified intrusions and geo-referenced these to the surface deformation that was  
621 produced. For sill emplacement, Galland (2012) noted the symmetrical up-doming of the  
622 initially flat experiment surface in response to the sill emplacement, with the complexity of  
623 the sub-surface intrusion that was later excavated being comparable to the complexity of the  
624 surface deformation it caused. The formation and growth of visible fractures, lateral and  
625 vertical displacement, and calculation of shear strain based on surface changes with time was  
626 mapped using DIC.

#### 627 ***6.1.3 Solidification and viscosity effects***

628 Experimental work has shown that the viscosity of the fluid within sheet intrusions can impact  
629 the geometry of dykes and sills as they propagate in their host material. Solidifying magma  
630 analogues used in dyke experiments include vegetable oil (Vegetaline), and viscous liquids  
631 such as golden syrup and honey (see Table 1). Solidification within dykes has been studied in



632 gelatine experiments (e.g. Taisne and Tait 2011, Figure 7d) and show a transition in  
633 propagation behaviour of the dyke tip from continuous to step-wise; with progressive stalling,  
634 inflation and then breakout due to breach of an insulated and relatively low viscosity fluid  
635 from the intrusion interior through a cooled margin. Chanceaux and Menand (2014; 2016)  
636 formed sills between gelatine layers by injecting solidifying Vegetaline directly into an  
637 interface (Figure 8e-f). They found that the sill tip region has the tendency to become  
638 segmented especially when the injected fluid is viscous or has become more viscous due to  
639 solidification.

## 640 **6.2 Numerical modelling of sheet intrusions**

641 Numerical models of sheet intrusions are often two-dimensional and adhere to physics-based  
642 principles which consider the coupled transport of a viscous fluid through a host rock that  
643 deforms and fractures. Additional complexities such as heat exchange with the surroundings,  
644 magma cooling and solidification, impact of mechanical layering of the host, local or regional  
645 stress perturbations and the presence of weak discontinuities such as faults or fractures are  
646 sometimes considered, though rarely simultaneously due to the increased complexity.

### 647 **Dyke propagation**

648 A comprehensive review by Rivalta et al. (2015) explores the state of knowledge regarding  
649 dyke propagation models that use: 1) Weertman theory (1971), where the dyke is modelled  
650 as a buoyant magma-filled fracture, 2) lubrication theory (Spence et al. 1987; Lister 1990),  
651 where the dyke propagation is controlled by the flow of magma, or 3) a combination of both.  
652 A commonly used numerical approach to study dyke propagation is the boundary element  
653 method (BEM) (e.g. Dahm 2000; Muller et al. 2001; Maccaferri et al. 2011) which considers  
654 the coupling between magma pressure and rock deformation, using analytical solutions for  
655 elementary dislocations to represent a pressurised, propagating crack. Dyke propagation in a  
656 stress field, controls on dyke trajectory and tendency to form sills have been well studied  
657 numerically (e.g. Maccaferri et al. 2011; Barnett and Gudmundsson 2014). Three-dimensional  
658 FEM models are rare as they require re-meshing of the entire domain and so are more  
659 computationally demanding than the two-dimensional BEM approach, where re-meshing  
660 requires only that new elements are added to the dyke tip (see Figure 9a). The future of  
661 numerical model approaches to study dyke propagation will need to move towards three-



662 dimensional simulations to account for the complexities that are apparent in field geology  
663 studies and geophysical surveys.

#### 664 **Sills and laccoliths**

665 Numerical models of sills and laccoliths are often static, two-dimensional and axisymmetric.  
666 They commonly consider the evolving intrusion geometry and surrounding deformation of  
667 the host material by idealising deformation of the rock overburden as bending a stack of thin  
668 elastic plates, following the approach outlined by Pollard and Johnson (1973). Bungler and  
669 Cruden (2011) expanded the thin elastic plate theory to include fracture propagation criteria,  
670 fluid flow and the weight of the magma to explain the progression of the intrusion geometry  
671 from a bell-shaped geometry to flat-top and steep sided laccolith to thin disc-like morphology  
672 of large mafic sills over time (Figure 9b). In comparison, Michaut (2011) models shallow  
673 magma intrusions using nondimensionalization of the flow equation to describe magma  
674 spreading beneath an elastic crust, finding that the characteristic intrusion length depends on  
675 the elastic properties of the overburden and the characteristic intrusion thickness depends  
676 on the magma properties and the injection rate. Galland and Scheibert's (2013) model  
677 accounts for axisymmetrical uplift both above and outside the intrusion, and it has recently  
678 been used to invert for laccolith dimensions and depth associated with surface deformation  
679 at Cordón Caulle volcano during a rhyolite eruption in 2011 (Castro et al. 2016). Additional  
680 complexities such as accounting for natural topography, tackling non-axisymmetric intrusion  
681 geometries, assessing the impact of inelastic deformation of the host (e.g. Scheibert et al.  
682 2017; see Figure 9c) and considering pressure variations within the intrusion result in a non-  
683 unique set of best-fit simulations when applying models.

#### 684 **6.3 Testing magma intrusion models**

685 There are several challenges that mean testing magma transport models is not  
686 straightforward. By their very nature, magma intrusions are sub-surface features and so  
687 cannot be directly observed during their formation or when they are active. Insight into active  
688 intrusion processes in nature is typically interpreted based on analysis of surface deformation  
689 thought to be related to magma movement, and in combination with seismic data that is  
690 inferred to result from intrusion-related rock fracturing. Due to these limitations, there is  
691 much discussion in the literature regarding how to model dykes, either as hydraulic fractures



692 or viscous indenters as described above, and how horizontal sheet intrusions (sills) relate to  
693 the construction of larger igneous bodies such as laccoliths and magma chambers.

694 Numerical models of a penny-shaped hydrofracture propagating in an infinite elastic material  
695 (e.g. Savitski and Detourney 2002) have been used to interpret the results of hydraulic  
696 fractures in gelatine experiments. Using measurements from gelatine experiments (e.g.  
697 intrusion dimensions, injection flux, fluid viscosity, host material Young's modulus and  
698 Poisson's ratio) it has been shown that dyke propagation occurs in a toughness-dominated  
699 regime, where the fracture properties of the host-material control the dynamics (e.g. Menand  
700 and Tait 2002). Recently this method has been applied to water-filled sill intrusions and  
701 similarly their growth was found to be better approximated by growth in a toughness-  
702 dominated regime, where a sill forms along an interface between layers and is fed by a dyke  
703 (Kavanagh et al. 2017). However, in some cases sill growth in gelatine experiments has been  
704 better explained by viscosity-controlled dynamics (e.g. Kavanagh et al. 2006; Chanceaux and  
705 Menand, 2016).

706 There is great potential to use analogue models and numerical models of magma intrusion in  
707 combination to assist the development of inversion methods to characterise magma intrusion  
708 geometry and depth in nature. The numerical models that calculate intrusion geometry and  
709 depth using ground deformation measurements such as GPS and InSAR at active volcanoes  
710 (e.g. Fukushima et al. 2005) could be tested on analogue models of magma intrusion where  
711 the volume, depth and geometry of the experimental dyke or sill is known. This comparison  
712 will enable the validation and improvement of inversion models, with the identification of any  
713 experiment parameters that are modelled well and those which are not to help guide future  
714 research for hazard assessment at active volcanoes.

## 715 **7.0 Lava lakes and lava domes**

### 716 **7.1 Lava lakes**

717 Lava lakes are effusions of lava either at the top of an open conduit (e.g. Halema'uma'u lava  
718 lake, Kilauea), or a ponded area of an active lava flow (e.g. Kilauea Iki 1959-1960, Kilauea,  
719 Hawaii (Richter et al. 1970)). There are several active lava lakes in the world, each with a range  
720 of hazards; from gas plumes and outpourings of lava, to explosions which could occur without  
721 warning.



722 **Surface morphology**

723 Techniques such as time-lapse photography have shown that lava lake surfaces in nature are  
724 highly dynamic parts of a volcanic system (Orr & Rea 2012), and spreading of the gradually  
725 cooling lava lake surface has been linked to convection in the underlying lake and conduit.  
726 Karlstrom & Manga (2006) used molten paraffin wax to study lava lake dynamics, monitoring  
727 the surface of the wax with infrared cameras. The wax surface was cooled before a partially  
728 submerged bar pulled the crust apart at a constant velocity along an incision in the wax  
729 surface. This formed zig-zag rifting morphologies reminiscent of structures described at  
730 natural lava lakes, and enabled the calculation of the spreading rate, crustal thickness and  
731 yield stress of the crust and thus the strength of the convective forces acting upon the  
732 underlying magma. Harris (2008) used numerical modelling to study convection of a molten  
733 lava lake fed by a conduit. In his models, an upwelling injection of hot, degassing, buoyant  
734 and less viscous magma rises through the conduit to the lava lake. Radiative heat loss and  
735 surface spreading then induces cooling and an increase in fluid density that causes down-  
736 welling of the magma, with the highest viscosity magma flowing back down the conduit. This  
737 model is supported by syrup analogue models of Beckett et al. (2011) where it was shown  
738 that different density fluids may flow past one another during exchange flow in the conduit.

739 **Surface level variations**

740 Fluctuations in lava lake level have been associated with gas exsolution. Witham et al. (2006)  
741 carried out a series of experiments that released air from a deep 'chamber' into a cuboidal  
742 conduit (1 x 1 x 18 cm) of water attached to an approximately cubic (14.1 x 14.1 x 15 cm) 'lava  
743 lake'. Gas was released into the base of the conduit using a compressor; this decreased the  
744 water-air density, causing the bubbly mixture to rise into the surface reservoir due to  
745 buoyancy, resulting in an increased lava lake level. Gas was then released from the water at  
746 the surface of the higher reservoir, progressively increasing the hydrostatic pressure.  
747 Eventually the hydrostatic pressure of degassed-water in the lake exceeded the pressure from  
748 below, preventing further rise of gas-rich water and resulting in collapse of the conduit, fluid  
749 flow back down into chamber and lowering of the lake level. These analogue experiment  
750 results show that rising lava lake levels in nature could be explained by periods of increased  
751 gas emission from the chamber through the conduit, and that decreases in lake level could



752 occur when the magma-static pressure in the overlying magma column exceeds the pressure  
753 of the rising magma.

## 754 **7.2 Lava Domes**

755 Lava domes are effusions of degassed, highly viscous, silica-rich magma that accumulate at  
756 volcanic vents. Their emplacement can cause the build-up of gas and pressure in the conduit,  
757 increasing the potential for explosive eruptions or the formation of pyroclastic density  
758 currents. Modelling lava dome emplacement and stability is key for identifying thresholds for  
759 collapse and therefore for assessing the potential risk of such events. Aspects of lava dome  
760 emplacement that have been studied in analogue experiments include morphological  
761 variations due to topography, magma rheology and the preservation of flow fabrics using  
762 magnetic fabrics.

### 763 **Dome morphology**

764 Analogue models of lava domes have largely focussed on the influence of lava rheology on  
765 dome morphology. Griffiths & Fink (1993) investigated the progressive spreading of lava  
766 domes by effusing liquid PEG 600 wax into a tank of cold sugar solution with a horizontal base.  
767 The temperature gradient between the wax and solution caused the onset of solidification,  
768 and the lava viscosity had a large influence on the morphology of the dome that was formed.  
769 Fink & Bridges (1995) found that pulsating the wax effusion and decreasing its temperature  
770 resulted in predominantly vertical growth of the dome rather than flow away from the vent,  
771 and so the length of lava domes could be explained primarily by variations in effusion rate.

772 Several lines of evidence suggest that lava dome rheology in nature is more complex than a  
773 simple temperature-dependent Newtonian fluid. Balmforth et al. (2000) carried out  
774 numerical simulations of lava dome growth and evolution using a Herschel-Buckley rheology.  
775 They found that the yield stress acting in the dome is important in determining dome  
776 morphology, however the combined effects of shear-thinning and yield stresses were difficult  
777 to distinguish. Experimentally, Griffiths and Fink (1997) used a PEG-kaolin mixture to study  
778 lava dome morphology with the kaolin powder converting the fluid from a temperature-  
779 dependent Newtonian fluid to a Bingham fluid. These analogue lava domes produced spines  
780 and irregular breakouts of wax (Figure 10a) due to the yield strength of the magma analogue.  
781 Lyman et al. (2004) used a similar mixture to investigate the impact of slope and effusion rate



782 on dome morphology. They found that contrasting dome morphologies (e.g., platy, spines,  
783 lobes) were associated with extrusion onto a surface at different slope angle, but that the  
784 effusion rate had the greatest impact on dome morphology. These results can be compared  
785 to lava dome morphologies in nature, such as Wilson Butte in California (Lyman et al., 2004),  
786 to calculate the effusion rate of prehistoric domes.

### 787 **Internal deformation**

788 Internal flow patterns within lava domes in nature has been inferred from crystalline and  
789 bubble fabrics within the crystalline lava, thus providing insight into the processes occurring  
790 within a dome during formation. Závada et al. (2009) studied magnetic fabric development  
791 within lava domes by effusing plaster of Paris seeded with magnetite particles from a point  
792 source, injecting with increasing pressure onto a deformable surface of sand (Figure 10b). The  
793 plaster of Paris and magnetite mixture behaves as a shear thinning fluid and was allowed to  
794 solidify once extruded. The solidified dome was then cut into slices and oriented samples  
795 drilled for analysis by applying Anisotropy of Magnetic Susceptibility (AMS) to quantify the  
796 direction and intensity of any fabric that was developed by the magnetite particles during the  
797 extrusion of the lava dome. They found more concentrated suspensions with higher viscosity  
798 created complex dome structures that had relatively steep sides, akin to lava domes  
799 commonly observed in nature.

## 800 **8.0 Volcanic flows**

801 Analogue and numerical modelling has been extensively applied to investigate the processes  
802 involved in the eruption, emplacement and deposition of hazardous flows such as lava flows,  
803 pyroclastic flows, lahars, debris flows and jökulhlaups (see Figure 1). The application of  
804 analogue modelling to volcanic flows has largely focused on understanding small-scale  
805 dynamic processes, such as granular interaction or controls on sedimentation, and the role of  
806 these processes on the large scale phenomena are commonly simulated in numerical models.  
807 Numerical models are driven by field observations and theoretical frameworks but also  
808 provide a stimulus for interpreting observations and recognizing new phenomena. Two types  
809 of modelling are used in the numerical simulation of volcanic flows; those applied to  
810 investigate the physical process behind flow emplacement, and those used in hazard  
811 assessment. Numerical models developed to reproduce volcanic phenomena are typically



812 deterministic and as such are more complex, have a large range of input parameters, and can  
813 have long run times. In comparison, models used for hazard assessment tend to simplify the  
814 physical problem by making several assumptions and characterising complex phenomena in  
815 terms of coefficients. As such, hazard assessment models are much more computationally  
816 efficient and can be used in real time.

## 817 **8.1 Lava flows**

### 818 ***8.1.1 Analogue models of lava flow dynamics***

819 The emplacement dynamics and morphology of lava flows has been investigated  
820 experimentally using a range of fluids (see Tables 1 and 2) and considering a spectrum of  
821 rheologies, from Newtonian fluids (e.g. glucose syrup; Stasiuk et al. 1993) to more complex  
822 fluids that account for cooling, crystallisation and develop a solidified crust during flow (e.g.  
823 PEG wax (e.g. Hallworth et al. 1987; Fink & Griffiths 1990; Gregg & Fink 1995). These  
824 experiments model variations in heat flux, thermal gradients and cooling on the temporal and  
825 spatial variation of lava flow viscosity, extrapolating on the impact these factors have on e.g.  
826 runout length and flow morphology.

827 Lavas have been modelled in the laboratory as a particle suspension, with experiments  
828 showing that increasing particle volume fraction (Soule & Cashman 2005; Castruccio et al.  
829 2014) and particle size (Del Gaudio et al. 2013) increases lava viscosity and can affect lava  
830 flow morphology. High concentration particle suspensions produce low flow velocities, shear  
831 localisation and subsequent break-up of the flow surface, causing transition from pahoehoe-  
832 like to 'a'a-like morphologies that are reminiscent of natural flows in nature (Soule & Cashman  
833 2005).

### 834 **Lava levees, crust formation and breakout**

835 Critical in the evolution of lava fields is the development of lava levees, crust formation and  
836 progressive breakout. This has been investigated in the laboratory using paraffin wax where  
837 the progressive cooling of the hot, liquid wax causes levees to form and channelization of the  
838 flow (Blake & Bruno 2000; Miyamoto et al. 2001; Nolan 2014). Crust formation over the  
839 cooling flow surface insulates the molten wax and creates tube-fed flows, and blockages or  
840 restrictions in the tube-fed flow of wax to the flow lead to flow inflation and eventually  
841 breakout from the crust. Blake & Bruno (2000) used PEG wax experiments to demonstrate



842 the link between lava effusion rate, lava viscosity and strength of the chilled crust which  
843 impacts how and where breakouts from lobate structures occur. Karlstrom & Manga (2006)  
844 used spreading paraffin wax experiments to study the morphological transition from  
845 pahoehoe to 'a'a flows due to breakouts from the cooled, spreading crust (also see section  
846 7.1 on lava lakes).

#### 847 **Substrate erosion**

848 Field observations of erosion channels within lava tubes suggest that assimilation of the lava  
849 substrate can occur when lava flows are emplaced with high heat flux or flow over substrate  
850 with a low melting temperature. Huppert and Sparks (1985) investigated the development  
851 of thermal erosion channels in komatiite lava flows by pouring hot water onto a slab of PEG  
852 1000 wax; Komatiite lavas are thought to have had unusually high heat flux, and so thermal  
853 erosion of their substrate is expected to have been an important process in the development  
854 of these ancient flows. Kerr (2001) used theoretical models alongside molten PEG 600 effused  
855 onto an inclined sheet of solid PEG 600 (Figure 11a) to investigate how the thermal profile of  
856 lava flows evolves both spatially and temporally. His experimental results agreed with the  
857 theoretical models which showed that there is a critical thickness range at which chilled  
858 margin formation at the base of the flow ceases and erosion begins, depending on the initial  
859 temperature of the lava; for basaltic lavas on Hawai'i, this range is 7.3 to 34 cm after a period  
860 of 0.21 to 4.6 days.

#### 861 **Flow indicators**

862 When studying ancient solidified flows in nature, crystal distribution and stretched bubbles  
863 have been used to infer flow direction. The preservation of flow indicators in solidified lavas  
864 was investigated in analogue experiments using layered viscous silicone to model internal  
865 strain within extruding and spreading fluids (Gilbert & Merle 1987). The experiments showed  
866 that in channelized flows, or at the base of a lobe, the lava flow trajectory indicators could be  
867 both parallel and perpendicular to each other in the upper portion of lobes. When applied to  
868 lava flows in nature, such observations can explain emplacement mechanisms and possibly  
869 account for variations in deformed bubble and crystal shape-preferred orientations  
870 compared to AMS fabrics in different parts of the flow (e.g. Caballero-Miranda et al. 2016).  
871 Solidification and development of columnar jointing in lava flows has been modelled using



872 corn starch slurries that are placed under heat lamps to allow the water to evaporate away  
873 (Goehring & Morris 2005; Müller 1998). The loss of water was used as an analogue for heat  
874 loss within lavas; as the starch dries out it shrinks, resulting in cracks forming and propagating  
875 through the material (Figure 11b). The morphology of the vertical columns formed within the  
876 analogue lava correlates well with the morphology of columns in natural lava lakes and  
877 ponded lava flows such as in Hawaii (Goehring et al. 2006; Müller 1998) or the Giant's  
878 Causeway in Northern Ireland (Goehring & Morris 2005). However, further rheological  
879 studies to understand better the material properties are needed to improve scaling these  
880 experiments to nature.

#### 881 **8.1.2 Numerical modelling**

882 Numerical models of lava flows have been applied to investigate the dynamics of lava flow  
883 emplacement, for example the controls on flow length. Lava flow emplacement models have  
884 been used to simulate edifice growth from the accumulation of multiple lava flows (Annen et  
885 al. 2001), the insulating properties of lava tubes (Keszthelyi 1995), cooling of pahoehoe lavas  
886 (Keszthelyi & Denlinger 1996) and formation of lava levées (Quareni et al. 2004). Lava flows  
887 have been modelled using a range of numerical techniques, from the simulation of physical  
888 process of emplacement using Navier Stokes equations with simplified equations of state, to  
889 probabilistic assessment of lava flow inundation. Particular emphasis has been on  
890 investigating the effects of rheology on flow behaviour. Robertson and Kerr (2012) analysed  
891 the effects of viscoplastic lava rheology on lava flow dynamics by modelling the flow as a  
892 Bingham fluid within a rectangular flow. Their results show that the formation of plug regions  
893 have a large impact on modelled flow velocities. Castruccio et al. (2014) apply the Herschel-  
894 Bulkley model to investigate the rheology and infer eruption source conditions, for example  
895 flow rate, of lava flows using observed lava flow dimensions and petrological and validate  
896 model results with analogue model results.

897 Numerical models are the main tool for hazard and risk assessment of lava flows, in particular  
898 inundation. For these purposes, simulated lava flows are emplaced over a DEM to predict the  
899 inundation pathways of flows. Cellular automata models are commonly used for hazard  
900 assessment (e.g. Miyamoto & Sasaki 1997; Crisci et al. 2004; Vicari et al. 2007; Connor et al.  
901 2012; Rongo et al. 2016) (Figure 11c). In these models, the area of interest is discretised into  
902 a regular grid of cells, with each cell having a finite number of states. In the case of lava flow



903 modelling, these states generally reflect the whether a cell has been inundated or not. In  
904 Connor et al. (2012), the probability of a cell being inundated is dependent on the relation  
905 between the elevation of the empty cell and the thickness of the lava in neighbouring cells.  
906 Such models assume a given volume is erupted, with this volume being distributed amongst  
907 the inundated cells. While these models do not provide insight into the physical process of  
908 lava flow emplacement, their simplicity and computational efficiency means that they can be  
909 run many times using, for example using Monte Carlo simulations, to produce probability  
910 assessments of inundated areas.

## 911 **8.2 Particle-laden flows**

912 Particulate-laden flows are one of the most hazardous phenomena associated with explosive  
913 volcanic eruptions. Pyroclastic density currents and lahars can impact areas hundreds of  
914 kilometres from source. Our understanding of pyroclastic density current and lahar processes  
915 is particularly reliant on numerical and analogue modelling, due to the hazardous nature of  
916 the phenomenon.

### 917 ***8.2.1 Pyroclastic density currents***

918 The term pyroclastic density current (PDC) encompasses a wide range of flows from dilute  
919 surges, to dense flows, block-and-ash flows and pumice flows; they represent a wide-ranging  
920 spectrum of flow behaviour from dense to dilute (Branney & Kokelaar 2002; Sulpizio & Dellino  
921 2008). Such flows occur as a mixture of particles and gas is emplaced as a gravity current  
922 which propagates down the slopes of a volcano and are related to, for example, collapse of a  
923 volcanic column or lava dome.

924 For the purposes of this overview, it is sufficient to consider a pyroclastic flow as divided into  
925 two main parts: a dense basal portion where movement is controlled by particle-particle  
926 interaction, and an overlying turbulent dilute region that is composed of ash and gas. It is not  
927 well understood how these distinct portions of the pyroclastic density current interact; this  
928 complexity and additional numerical challenges, have resulted in analogue and numerical  
929 modelling techniques typically representing either the lower dense portion of the flow (e.g.  
930 the flow simulation software TITAN2D) or the dilute portion of the flow (e.g. Bursik & Woods  
931 1996; Andrews & Manga 2011).



932 **Analogue models of PDCs**

933 Some of the first analogue experiments to investigate controls on pyroclastic density current  
934 propagation involved the injection of dense, sometimes particle laden, fluid into less dense  
935 fluid (Carey et al. 1988; Huppert et al. 1986; Sparks et al. 1993; Woods & Bursik 1994; Woods  
936 & Caulfield 1992). In the example of Carey et al. (1988), buoyant plumes were produced by  
937 injection of particle laden freshwater into saline water. Flows formed when the particle  
938 concentration of the injected fluid was large such that the density difference with the ambient  
939 was negligible, leading to collapse of the plume. Woods and Bursik (1994), specifically focused  
940 on the movement of flows on slopes and their interaction with topographic barriers (Figure  
941 12a). In this example, dense fluid was made of a mixture of methanol and ethylene glycol  
942 (MEG) which was injected or released into water. Such experiments provided information on  
943 the control of entrainment on flow density, and controls of topography on both entrainment  
944 and sedimentation from a flow. More recently analogue experiments have considered the  
945 effect of interstitial pore pressure on flow motion (Figure 12b) (Roche 2012; Rowley et al.  
946 2014) and the controls on co-ignimbrite plume formation from dilute flows using talc to  
947 represent fine grained ash particles (Andrews & Manga 2011; 2012). As for all analogue  
948 experiments, scaling is a key issue when designing experiments to simulate explosive eruptive  
949 phenomena. However, over the past 5 – 10 years, significant effort has focused on the  
950 development of so-called ‘large-scale’ experimental setups to overcome this (Figure 12c)  
951 (Dellino et al. 2007; Lube et al. 2015; Valentine et al. 2015) and try to more accurately  
952 reproduce observed phenomena. Such modelling also allows the use of natural eruptive  
953 pyroclastic materials to more accurately reproduce the physical dynamics, states and  
954 relations that occur within real flows.

955 **PDC Numerical models**

956 Numerical models that describe either the dilute- or dense- end member flow are typically  
957 depth averaged, and solve equations for conservation of mass, momentum and thermal  
958 energy (e.g. Bursik and Woods 1996). Such models are also steady state, and therefore do not  
959 account for changes in flow behaviour with time. An example of a numerical model that has  
960 been developed to account for both the turbulent upper layer and the dense layer is the  
961 transient model of Doyle et al. (2008). In this model, the dilute current is described by depth



962 averaged, isothermal, continuum conservation equations, while the basal flow is modelled as  
963 a granular avalanche of constant density.

964 In addition to the production of separate models to account for different physical processes,  
965 numerical models of varying complexity also exist. Numerical models have been developed  
966 that consider dilute particle-laden gravity currents (e.g. Bursik & Woods 1996; Dade &  
967 Huppert 1996) to calculate properties such as velocity, temperature and density of the flows.  
968 These calculations have a small number of parameters and as such involve a number of  
969 simplifications, allowing parametric studies to be conducted to understand the control of  
970 inputs on the modelled outputs. The advancement of computational efficiency has enabled  
971 the development of supercomputer calculations, solving full Navier-Stokes equations for  
972 flows and fountains (Valentine et al. 1992; Neri & Dobran 1994; Esposti Ongaro et al. 2012).  
973 These are elaborate computer codes, incorporating a large number of input parameters, and  
974 solving for a number of different phases, for example fluid (magmatic and atmospheric gases)  
975 and particles of different sizes and density simultaneously (Figure 12d). While numerical  
976 studies of pyroclastic density currents still largely follow these two strands, open source  
977 computational fluid dynamics programs (e.g. MFix and OpenFOAM) are being increasingly  
978 used to capture the multiphase behaviour that occurs within these volcanic flows. A  
979 comprehensive overview of the numerical models describing pyroclastic density currents is  
980 provided in Dufek (2016).

### 981 **8.2.2 Lahars**

982 Primary lahars form when an eruption causes melting of ice overlying the volcano, and  
983 eruptive products mix with melt water to produce high-density mixtures of water and debris.  
984 Secondary lahars form as debris emitted by an eruption is mobilized after deposition, usually  
985 in relation to heavy rainfall between eruptive events.

986 Similarly to pyroclastic density currents, lahars can be described by two end members: stream  
987 flows and debris flows, but with an intermediate flow type called hyper-concentrated flows.  
988 Flow type can vary within an individual event both spatially and temporally, in association  
989 with changes in channel and underlying topography (e.g. Manville et al. 2013). Definition of  
990 lahar flow type is dependent on the concentration of particles, with stream flows  
991 representing those with low particle concentrations and debris flows with high particle



992 concentration. The flow end members have very different rheology, and as a result the  
993 application of both analogue and numerical modelling techniques are affected by similar  
994 challenges to those for pyroclastic density current.

995 Lahar analogue experiments have largely considered debris flows, i.e. those with high particle  
996 concentration. As for pyroclastic density currents, both small (metre) and large (tens of  
997 meters) scale analogue experiments have been conducted. Iverson (2015) showed that  
998 experiments of debris flows are particularly susceptible to scaling issues. The USGS has  
999 developed a 95 metre long flume that allows the release and flow of  $10\text{ m}^3$  of water-saturated  
1000 sediment onto a bed with variable roughness to closely mimic conditions in natural debris  
1001 flows (Iverson et al. 2010; 2011).

1002 In comparison to the number of models available to simulate the emplacement of pyroclastic  
1003 density currents, there are relatively few models that simulate lahars. Numerical modelling  
1004 of lahar dynamics is non-trivial due to spatial and temporal variation in flow behaviour, for  
1005 example rheology (see Manville et al. 2013). Perhaps the most commonly used numerical  
1006 model to simulate lahar emplacement is LAHARZ (Schilling 2014), a computational model that  
1007 uses empirical relations of past inundation events to forecast inundation for a given future  
1008 event. More complex numerical models applied to lahars include a version of TITAN2D that  
1009 accounts for both particles and fluids (Pitman et al. 2003; Williams et al. 2008), the  
1010 commercial hydraulic model Delft3D (Carrivick et al. 2008), GIS-based models (Darnell et al.  
1011 2012), and application of models more typically applied to water floods, e.g. LISFLOOD. No  
1012 single model can account for the all the different phenomena described above, due to the  
1013 complex interactions between the solid and liquid phases. As such, research into the rheology  
1014 of lahars is required to provide a description of the underlying physics to be utilized in  
1015 numerical models.

## 1016 **9.0 Volcanic plumes**

1017 Much of our current understanding of plume dynamics can be traced back to the 1950's and  
1018 the work of Morton et al. (1956) (see Figure 3c). While not focusing specifically on volcanic  
1019 plumes, their study has been the basis for much of the subsequent research into volcanic  
1020 plumes using analogue modelling and numerical models to reproduce behaviour observed in  
1021 nature.



## 1022 **9.1 Analogue models of volcanic plumes**

1023 Traditional analogue modelling of volcanic plumes has involved the injection of a less dense  
1024 fluid (e.g. fresh water or methanol) into a tank of denser fluid (e.g. saline fluid or ethylene-  
1025 glycol respectively). The difference in densities between the two fluids allows the less dense  
1026 fluid to rise through the dense fluid, reproducing those characteristics associated with  
1027 buoyancy plume rise (see Figure 13a Carey et al. 1988). Injection into a stratified fluid enables  
1028 not only modelling of plume rise, but also the dynamics of plume spreading once the injected  
1029 mixture reaches neutral density (e.g. Carey et al. 1988). Variation in the injection rate  
1030 provides first order information on plume dynamics, and in particular on the controls on  
1031 column collapse (Woods & Caulfield 2007; Kaminski et al. 2005). In some examples, the  
1032 injected fluid is particle laden to investigate the additional effect of particle sedimentation  
1033 and re-entrainment on buoyant columns (Ernst et al. 1994 and Carey et al. 1988), such that  
1034 experimental observations can be related to those seen in ash fallout deposits in the field. In  
1035 particular, Ernst et al. (1994) looked at the effect of wind on volcanic plumes, reproducing the  
1036 bifurcation of the plume. These experiments are based around buoyant theory, and therefore  
1037 ignore the processes occurring in the jet region of the plume, where dynamics are controlled  
1038 by the upward velocity of material as it is ejected from vent. Such laboratory experiments  
1039 underlie the one-dimensional numerical models currently used to investigate volcanic plume  
1040 behaviour and inform inputs for ash dispersal models widely used today.

1041 A key issue with analogue modelling of volcanic plume dynamics is scaling, particularly when  
1042 considering that plumes in nature are injected into a stratified and turbulent atmosphere and  
1043 are affected by local weather patterns. To account for such scaling issues, macro scale  
1044 experiments are increasingly applied to investigate eruption processes (e.g. Dellino et al.  
1045 2014; Figure 13b). These experiments, which often use natural materials, have enabled  
1046 analysis of the effect of vent conditions and processes on subsequent eruption behaviour,  
1047 and in particular have been used to estimate the rate at which air is entrained into the rising  
1048 plume, a key input parameter for numerical modelling of plume rise (Costa et al. 2016).

## 1049 **9.2 Numerical models of volcanic plumes**

1050 Numerical models of volcanic plumes serve two main purposes: 1) to provide input  
1051 information (for example plume height and mass flux of ash into the atmosphere) for ash-



1052 dispersal models, and 2) to investigate the controls on these parameters. Two types of  
1053 numerical model are available; one-dimensional (integral) models and multicomponent  
1054 multiphase three-dimensional models.

### 1055 ***9.2.1 One-dimensional numerical models of volcanic plumes***

1056 One-dimensional models (Figure 13c) are commonly used for defining source parameters for  
1057 ash dispersal models, largely because they are computationally inexpensive, and results can  
1058 be acquired quickly. These models account for conservation of mass, momentum and energy,  
1059 and are largely based around the model developed by Morton et al. (1956), with the  
1060 constituent equations modified for application to the volcanic example by Wilson and Walker  
1061 (1987), Sparks (1986) and Woods (1988). Since the 2010 eruption of Eyjafjallajökull, there has  
1062 been increased emphasis on development of models that are able to account for the effects  
1063 of wind on a rising plume (e.g. Woodhouse et al. 2013; Degruyter & Bonadonna 2013). The  
1064 models assume that the emitted gas and particles are in dynamic and thermal equilibrium; an  
1065 approximation that is reasonable for dilute, fine grained plumes but is less appropriate in the  
1066 jet part of the plume. To address this, Kaminski et al. (2005) and Carazzo et al. (2008)  
1067 developed a modified Reynolds number dependent entrainment law to account for the  
1068 negative buoyancy in the jet portion of the plume.

1069 Entrainment coefficients are key inputs for plume models, and these parameters have been  
1070 the focus of much research in recent years. Entrainment in one-dimensional models is  
1071 captured using two additive entrainment parameters, one accounting for radial entrainment  
1072 associated with the incorporation of ambient air by turbulent eddies at the plume edge, and  
1073 the second accounting for the effect of wind on air entrainment. The first coefficient has been  
1074 well defined using observations from analogue experiments of turbulent jets (Kaminski et al.  
1075 2005). In comparison, the second coefficient is still relatively poorly constrained, and requires  
1076 more targeted experiments, both analogue and using three-dimensional numerical models.

### 1077 ***9.2.2 Three-dimensional numerical models of volcanic plumes***

1078 While modifications to one-dimensional axisymmetric models have been relatively minor  
1079 over the past 60 years, there have been great advancements in the application of more  
1080 complex three-dimensional models. Great improvements in computational efficiency have  
1081 enabled the development of increasingly sophisticated models (e.g. Figure 13d; Cerminara et



1082 al. 2016). These models are able to account for a larger range of particle sizes, over much  
1083 greater scales than possible previously (e.g. Woods 1988), and are increasingly used to  
1084 investigate the assumptions utilized in one-dimensional models (Suzuki & Koyaguchi 2015).  
1085 Three-dimensional models are increasingly able to account for small-scale processes, for  
1086 example turbulence and microphysics (Cerminara et al. 2016; Herzog & Graf 2010; Suzuki &  
1087 Koyaguchi 2012), on plume behaviour. Within such three-dimensional models, gas and ash  
1088 phases are treated as intermingled continua, accounting for mass and momentum transfer  
1089 between the phases. Such models are utilized in an experimental way, and provide detailed  
1090 insights into plume processes. Despite these great advances in three-dimensional numerical  
1091 modelling capabilities, there is still a large amount to learn about the relative motion of  
1092 particles and gas. In addition, further detailed laboratory analysis is required to understand  
1093 variation of entrainment under real atmospheric conditions, particularly when under the  
1094 influence of wind. From a practical point of view, while results are likely more accurate than  
1095 those from one-dimensional models, the application of three-dimensional numerical models  
1096 is still limited by computational efficiency, and their results may take many weeks to process  
1097 and interpret.

## 1098 **10.0 Ash dispersal models**

1099 Perhaps the most disruptive aspect of an explosive eruption in terms of geographical scale is  
1100 the injection of volcanic ash into the atmosphere. Ash can be transported hundreds to  
1101 thousands of kilometres downwind from the source, impacting aviation and downwind  
1102 communities and infrastructure. Ash dispersal is controlled by a complex relationship  
1103 between volcanic source and atmospheric conditions; proximal to source dispersion is almost  
1104 completely controlled by the characteristics of the eruption, while distally, atmospheric  
1105 physics take over. Given the potential for significant disruption over long timescales, large  
1106 amounts of research has focused on the mechanisms controlling both ash dispersal and  
1107 deposition.

### 1108 **10.1 Analogue models of ash dispersal**

1109 Analogue modelling of ash transport in the atmosphere predominantly relates to near source  
1110 processes and to investigating controls on sedimentation. A number of studies have focused  
1111 on the intrusion of the volcanic plume as a buoyancy driven gravity current (e.g. Didden &



1112 Maxworthy 1982; Ivey & Blake 1985; Bursik et al. 1992; Kotsovinos 2000) into the  
1113 atmosphere. In these examples, a dense fluid is injected into a stratified fluid and the less  
1114 dense fluid rises through the dense fluid until it reaches its level of neutral buoyancy and  
1115 begins to spread laterally.

1116 A considerable number of experiments have focused on the physical controls on  
1117 sedimentation, and constraining parameters such as particle terminal settling velocity.  
1118 Koyaguchi et al. (2009) specifically focused on the effects of turbulence on particle dispersion  
1119 in the atmosphere by mixing spherical glass-bead particles in water with various intensities of  
1120 turbulence and measuring the spatial distribution and temporal evolution of the particle  
1121 concentration. These experiments provide insight into the settling behaviour of particles  
1122 within a turbulent regime, with results providing information on how particles are dispersed  
1123 during an eruption. Particle terminal settling velocity is estimated by dropping particles with  
1124 well-constrained characteristics through a fluid of a known density and viscosity (E.g.  
1125 Dioguardi et al. 2016). Analogue experiments have been used to quantify the effect of the  
1126 interactions between particles, but also particle-fluid interaction, on sedimentation (Del Bello  
1127 et al. 2017), by releasing different volume fractions of ash at variable discharge rates through  
1128 a chamber. Particle settling behaviour was captured using high-speed cameras, which showed  
1129 a large increase in settling rate with increase in particle volume fraction. The results were  
1130 validated by numerical simulation of particle behaviour. Manzella et al. (2015) also looked at  
1131 the effect of volume fraction of ash on settling behaviour, reproducing the gravitational  
1132 instabilities noted in field observations by mixing high concentrations of ash into water.  
1133 Finally, significant research has focused on how different particles interact with each, in  
1134 particular in relation to the formation of particle aggregates (Mueller et al. 2016). In such  
1135 example, as particles are released into a tank, and their sticking efficiency is measured using  
1136 high-speed camera imaging.

## 1137 **10.2 Numerical models of ash dispersal**

1138 Dispersal models are used to simulate the dispersal of particulate matter and gases during a  
1139 volcanic eruption, and in comparison to analogue models, generally focus on more distal  
1140 dispersal. In the case of particulate matter, the dispersion models have two main roles; to  
1141 forecast the dispersion of ash during a volcanic eruption, and to reproduce ancient eruptions  
1142 by fitting model results to observed deposit distributions. Numerical modelling of volcanic



1143 ash in the atmosphere requires the definition of three components (Folch 2012): 1) the source  
1144 describing the emission of particles and gas in the atmosphere, 2) an atmospheric model  
1145 (typically offline, providing information at fixed locations at regular time intervals) describing  
1146 the physical characteristics of the environment into which the plume is injected, and 3) the  
1147 transport model which describes how the particles are transported.

1148 Two main types of numerical models exist: a) buoyancy models that consider near source  
1149 plume characteristics, assume intrusion of the ash as a buoyant current and simulate the  
1150 deposition of coarse ash, and b) advection-diffusion ash transport models (Folch 2012).  
1151 Buoyant plume models describe the horizontal intrusion of volcanic plumes into the  
1152 atmosphere as a gravity current (Bursik et al. 1992; Baines et al. 2008; Suzuki & Koyaguchi  
1153 2009; Johnson et al. 2015). They are capable of reproducing both upwind dispersal (e.g.  
1154 Baines et al. 2008) and plume thickness variation (Johnson et al. 2015, which are key  
1155 considerations when assessing hazard to aviation. However, the majority of ash models  
1156 utilized to predict ash transport in the atmosphere are based on the advection of particles by  
1157 atmospheric winds, and the diffusion of ash by atmospheric turbulence (Folch 2012). A  
1158 number of different types of such tephra transport and dispersal models exist, and a  
1159 comprehensive review is provided in Bonadonna et al. (2011) and Folch (2012); they are  
1160 favoured as they are computationally efficient, allowing results in the order of 10's of  
1161 minutes. Transport models are typically Eulerian, solving for variable particles at fixed  
1162 locations, or Lagrangian, calculating the trajectories of a parcel of 'particles' and computing  
1163 mass concentration by averaging over the background. Advection-diffusion models predict  
1164 ash dispersion through the action of vertical wind shear, which can disperse ash in different  
1165 directions at different altitudes. Their results are therefore highly dependent on the wind field  
1166 that is used.

1167 Characterization of depositional processes is crucial for interpreting volcanic deposits,  
1168 however these are only accounted for in numerical models to a limited extent. Recent  
1169 advances in numerical modelling have aimed to incorporate the effects of aggregation (Folch  
1170 et al. 2016) and buoyancy forces (Costa et al. 2013) on plume dispersal. Attempts to include  
1171 aggregation in simulations are somewhat simplistic and are generally conducted by fixing a  
1172 priori input grainsize distributions rather than accounting for the physics of the process (e.g.  
1173 Cornell et al. 1983).



1174 **11.0 Perspectives and Conclusions**

1175 This review provides an overview of the development of modelling in volcanology, describing  
1176 some of the first experiments carried out using analogue materials and the development of  
1177 numerical models to describe volcanic phenomenon. It has not been possible to consider all  
1178 aspects of the volcanic system in detail meaning that some important research will  
1179 undoubtedly not be included here. By focusing on sub-surface processes such as magma flow,  
1180 magma chamber development and magma intrusion, and extrusive processes such as the  
1181 development of hazardous flows, volcanic plumes and ash dispersal we have identified  
1182 emerging lines of thought and make four suggestions listed below that point towards the  
1183 future of modelling in volcanology.

1184 1. Increased interaction between analogue and numerical modelling communities

1185 There is great potential to improve the interaction between analogue and numerical  
1186 modelling communities, and to develop iterative processes using both techniques to test  
1187 against data derived from nature. Scaled laboratory experiments allow us to observe and  
1188 understand physical processes and test basic assumptions; and in parallel with this, numerical  
1189 simulations model and enable the quantification of processes that are too complex, too large  
1190 or last too long to be reproduced in the lab. The approaches are therefore highly  
1191 complementary. Adopting an engineering approach of systematically testing a numerical  
1192 simulation against the expected outcomes from a scaled analogue experiment would be a  
1193 positive step towards integrating these techniques.

1194 A number of studies of volcanic processes using numerical modelling (e.g. Scollo et al. (2008)  
1195 and Costa et al. (2016), and references therein) have shown how statistical techniques such  
1196 as uncertainty quantification and sensitivity analysis can be used to systematically evaluate  
1197 numerical models. The effect model input uncertainties have on the model outputs, and the  
1198 interaction of inputs within the model, is evaluated highlighting important  
1199 interdependencies. A key advancement in the application of numerical techniques is the way  
1200 in which they are applied with the use of ensemble modelling, where several different models  
1201 are applied to investigate the most likely outcomes. Such techniques are well used in other  
1202 sciences, for example in climate studies, but have yet to be systematically utilized in  
1203 volcanology.



1204        2. Implement benchmarking exercises and systematic review

1205        Analogue and numerical models in volcanology study processes that span the crust-mantle  
1206        interface into the stratosphere and cross orders of magnitude in time and space. The  
1207        objectives of any model are carefully defined, and different approaches need to be  
1208        considered depending the application. Models that are developed in the laboratory or  
1209        numerically are ultimately limited by the conceptual models they simulate, and these will be  
1210        based upon diverse data sources such as geochemistry, petrology, geophysics, real-time  
1211        observations and field geology. Referring the model outputs back to known outcomes based  
1212        on observations from nature is a fundamental step that ensures the model boundary  
1213        conditions are well informed.

1214        Benchmarking has been employed for modelling tectonic processes (e.g. Schreurs et al. 2006)  
1215        and similar exercises would be of benefit in volcanology. A recent benchmarking operation  
1216        of numerical modelling of volcanic behaviour was undertaken by Costa et al (2016) and  
1217        demonstrated the benefits of this but was limited as the models tested against each other all  
1218        have the same underlying assumptions. Further testing against observed eruptions would  
1219        allow continued examination of the validity of these assumptions. However, similar exercises  
1220        are needed for analogue modelling in volcanology.

1221        3. Periodic review of conceptual modelling framework

1222        In many cases the conceptual models of physical processes in volcanology are constantly  
1223        evolving, and new insights and developments that come from advancements in formative  
1224        fields have the potential to revolutionise the framework upon which the analogue and  
1225        numerical models are based. For example, in the case of magma chambers there is current  
1226        discussion regarding their formation (see Sparks and Cashman 2017 for a review) and  
1227        relationship with plutonic bodies (see Lundstrom and Galzner (2016) and papers in the same  
1228        Volume for discussions). Advancement in geochronology has meant that high resolution  
1229        dating of ancient magma bodies is now possible, and has since demonstrated that in at least  
1230        certain case studies the magma was emplaced over a timescale that is longer than the thermal  
1231        lifetime such large magma masses (Galzner et al. 2004). Consequently, plutons are now  
1232        thought to have been accreted by the in-situ amalgamation of many small increments and



1233 the relationship between magma chambers and plutons and the numerical and analogue  
1234 models that are used to study them are being revisited.

1235 4. Utilise a multidisciplinary approach

1236 Volcanology as a discipline has significantly benefitted from the understanding and  
1237 technological advancements across diverse fields, from engineering to material science. Fluid  
1238 dynamics theory has been applied to study all parts of the volcanic system, for example plume  
1239 theory that was initially developed to study factory emissions has been applied to the  
1240 development of ash plumes but also the injection of hot, buoyant magma into the base of a  
1241 magma chamber. The combination of field observations with geophysical analysis and  
1242 monitoring techniques has enabled construction of informed conceptual models and  
1243 hypotheses; these have then been tested in the laboratory using analogue experiments or  
1244 computationally using numerical modelling. It is clear that the most significant advancements  
1245 have come from utilising a multidisciplinary approach, and this needs to be developed further  
1246 in order to push the frontiers of volcanology.



1247 **Acknowledgements**

1248 JK and SM acknowledge support from the University of Liverpool, and JK thanks Catherine  
1249 Annen for her valuable input and helpful discussions during manuscript preparation. SE  
1250 acknowledges Mattia de' Michieli Vitturi and Fabio Dioguardi for helpful discussion. Many  
1251 thanks to Kay Lancaster for drafting Figure 1 and to Prokop Zavada for providing images used  
1252 in Figure 10. Susanne Buitter and Andreas Lang are thanked for their editorial support.

1253 **References**

- 1254 Abdelmalak, M.M. et al., 2012. Fracture mode analysis and related surface deformation  
1255 during dyke intrusion Results from 2D experimental modelling. *Earth and Planetary*  
1256 *Science Letters*, 359-360(C), pp.93–105.
- 1257 Andrews, B.J. & Manga, M., 2011. Effects of topography on pyroclastic density current runout  
1258 and formation of coignimbrites. *Geology*, 39(12), pp.1099–1102.
- 1259 Andrews, B.J. & Manga, M., 2012. Experimental study of turbulence, sedimentation, and  
1260 coignimbrite mass partitioning in dilute pyroclastic density currents. *Journal of*  
1261 *Volcanology and Geothermal Research*, 225-226, pp.30–44.
- 1262 Annen, C., 2009. From plutons to magma chambers: Thermal constraints on the accumulation  
1263 of eruptible silicic magma in the upper crust. *Earth and Planetary Science Letters*, 284(3-  
1264 4), pp.409–416.
- 1265 Annen, C., Lénat, J.F. & Provost, A., 2001. The long-term growth of volcanic edifices:  
1266 numerical modelling of the role of dyke intrusion and lava-flow emplacement. *Journal of*  
1267 *Volcanology and Geothermal Research*, 105, pp.263–289.
- 1268 Annen, C., Blundy, J.D. & Sparks, R.S.J., 2006a. The Genesis of Intermediate and Silicic Magmas  
1269 in Deep Crustal Hot Zones. *Journal of Petrology*, 47(3), pp.505–539.
- 1270 Annen, C., Blundy, J. & Sparks, R.S.J., 2006b. The sources of granitic melt in Deep Hot Zones.  
1271 *Transactions of the Royal Society of Edinburgh: Earth Sciences*, 97, pp.297–309.
- 1272 Annen C. et al., 2008. Conditions for the growth of a long-lived shallow crustal magma  
1273 chamber below Mount Pelee volcano (Martinique, Lesser Antilles Arc). *Journal of*  
1274 *Geophysical Research: Solid Earth*, 113(B7).
- 1275 Annen, C. et al., 2014. Quantification of the Intrusive Magma Fluxes during Magma Chamber  
1276 Growth at Soufriere Hills Volcano (Montserrat, Lesser Antilles). *Journal of Petrology*,  
1277 55(3), pp.529–548.
- 1278 Annen, C. et al., 2015. Construction and evolution of igneous bodies: Towards an integrated  
1279 perspective of crustal magmatism. *Lithos*, 230(C), pp.206–221.
- 1280 Bagdassarov, N. & Pinkerton, H., 2004. Transient phenomena in vesicular lava flows based on  
1281 laboratory experiments with analogue materials. *Journal of Volcanology and Geothermal*  
1282 *Research*, 132(2-3), pp.115–136.
- 1283 Baines, P.G., Jones, M.T. & Sparks, R.S.J., 2008. The variation of large-magnitude volcanic ash  
1284 cloud formation with source latitude. *Journal of Geophysical Research*, 113(D21),  
1285 p.D21204.
- 1286 Balmforth, N.J. et al., 2000. Visco-plastic models of isothermal lava domes. *Journal of Fluid*  
1287 *Mechanics*, 403, pp.37–65.
- 1288 Barnett, Z.A. & Gudmundsson, A., 2014. *Journal of Volcanology and Geothermal Research*.



- 1289 Journal of Volcanology and Geothermal Research, 281(C), pp.1–11.
- 1290 Beckett, F.M. et al., 2011. An experimental study of low-Reynolds-number exchange flow of  
1291 two Newtonian fluids in a vertical pipe. *Journal of Fluid Mechanics*, 682, pp.652–670.
- 1292 Benn, K., Odonne, F. & de Saint Blanquat, M., 1998. Pluton emplacement during transpression  
1293 in brittle crust: New views from analogue experiments. *Geology*, 26(12), p.1079.
- 1294 Bhattacharji, S. & Smith, C.H., 1964. Flowage differentiation. *Science*, 145, pp.150–153.
- 1295 Blake, S. & Bruno, B.C., 2000. Modelling the emplacement of compound lava flows. *Earth and*  
1296 *Planetary Science Letters*, 184(1), pp.181–197.
- 1297 Bonadonna, C. et al., 2011. Future developments in modelling and monitoring of volcanic ash  
1298 clouds: outcomes from the first IAVCEI-WMO workshop on Ash Dispersal Forecast and  
1299 Civil Aviation. *Bulletin of volcanology*, 74(1), pp.1–10.
- 1300 Bons, P.D. et al., 2014. Layered intrusions and traffic jams. *Geology*, 43(1), pp.71–74.
- 1301 Branney, M.J. & Kokelaar, B.P., 2002. Pyroclastic density currents and the sedimentation of  
1302 ignimbrites, Geological Society Memoir 27. Geological Society of London, 152 pp.
- 1303 Bunger, A.P. & Cruden, A.R., 2011. Modeling the growth of laccoliths and large mafic sills: Role  
1304 of magma body forces. *Journal of Geophysical Research*, 116(B02203),  
1305 pp.doi:10.1029/2010JB007648.
- 1306 Bursik, M.I. & Woods, A.W., 1996. The dynamics and thermodynamics of large ash flows.  
1307 *Bulletin of volcanology*, 58(2-3), pp.175–193.
- 1308 Bursik, M.I., Carey, S.N. & Sparks, R., 1992. A gravity current model for the May 18, 1980  
1309 Mount St. Helens plume. *Geophysical Research Letters*, 19(16), pp.1663–1666.
- 1310 Caballero-Miranda, C.I. & Alva-Valdivia, L.M., 2016. Vertical AMS variation within basalt flow  
1311 profiles from the Xitle volcano (Mexico) as indicator of heterogeneous strain in lava flows.  
1312 *Journal of Volcanology and Geothermal Research*, 311, pp.9–28.
- 1313 Carazzo, G., Kaminski, E. & Tait, S., 2008. On the rise of turbulent plumes: Quantitative effects  
1314 of variable entrainment for submarine hydrothermal vents, terrestrial and extra  
1315 terrestrial explosive volcanism. *Journal of Geophysical Research*, 113(B9), p.B09201.
- 1316 Carey, S.N., Sigurdsson, H. & Sparks, R.S.J., 1988. Experimental studies of particle-laden  
1317 plumes. *Journal of Geophysical Research*, 93(B12), pp.15314–15328.
- 1318 Carrivick, J.L., Manville, V. & Cronin, S.J., 2008. A fluid dynamics approach to modelling the  
1319 18th March 2007 lahar at Mt. Ruapehu, New Zealand. *Bulletin of volcanology*, 71(2),  
1320 pp.153–169.
- 1321 Castro, J.M. et al., 2016. Rapid laccolith intrusion driven by explosive volcanic eruption.  
1322 *Nature Communications*, 7, pp.1–7.



- 1323 Castruccio, A., Rust, A.C. & Sparks, R., 2014. Assessing lava flow evolution from post-eruption  
1324 field data using Herschel–Bulkeley rheology. *Journal of Volcanology and Geothermal*  
1325 *Research*, 275, pp.71–84.
- 1326 Castruccio, A., Rust, A.C. & Sparks, R.S.J., 2010. Rheology and flow of crystal-bearing lavas:  
1327 Insights from analogue gravity currents. *Earth and Planetary Science Letters*, 297(3-4),  
1328 pp.471–480.
- 1329 Cerminara, M., Ongaro, T.E. & Neri, A., 2016. Large eddy simulation of gas–particle kinematic  
1330 decoupling and turbulent entrainment in volcanic plumes. *Journal of Volcanology and*  
1331 *Geothermal Research*, 326, pp.143–171.
- 1332 Chanceaux, L. & Menand, T., 2014. Solidification effects on sill formation: An experimental  
1333 approach. *Earth and Planetary Science Letters*, 403(C), pp.79–88.
- 1334 Chanceaux, L. & Menand, T., 2016. The effects of solidification on sill propagation dynamics  
1335 and morphology. *Earth and Planetary Science Letters*, 442, pp.39–50.
- 1336 Cimarelli, C. et al., 2011. Rheology of magmas with bimodal crystal size and shape  
1337 distributions: Insights from analog experiments. *Geochemistry Geophysics Geosystems*,  
1338 12(7), pp.DOI: 10.1029–2011GC003606.
- 1339 Coleman, D.S., Gray, W. & Glazner, A.F., 2004. Rethinking the emplacement and evolution of  
1340 zoned plutons: Geochronologic evidence for incremental assembly of the Tuolumne  
1341 Intrusive Suite, California. *Geology*, 32(5), pp.433–436.
- 1342 Connor, L.J., Connor, C.B., Meliksetian, K. and Savov, I., 2012. Probabilistic approach to  
1343 modeling lava flow inundation: a lava flow hazard assessment for a nuclear facility in  
1344 Armenia. *Journal of Applied Volcanology*, 1(1), p.3.
- 1345 Cornell, W., Carey, S. & Sigurdsson, H., 1983. Computer simulation of transport and  
1346 deposition of the Campanian Y-5 ash. *Journal of Volcanology and Geothermal Research*,  
1347 17, pp.89–109.
- 1348 Corti, G., Moratti, G. & Sani, F., 2005. Relations between surface faulting and granite  
1349 intrusions in analogue models of strike-slip deformation. *Journal of Structural Geology*,  
1350 27(9), pp.1547–1562.
- 1351 Costa, A. et al., 2016. Results of the eruptive column model inter-comparison study. *Journal*  
1352 *of Volcanology and Geothermal Research*, 326, pp.2–25.
- 1353 Costa, A., Folch, A. & Macedonio, G., 2013. Density-driven transport in the umbrella region  
1354 of volcanic clouds: Implications for tephra dispersion models. *Geophysical Research*  
1355 *Letters*, 40(18), pp.4823–4827.
- 1356 Crisci, G.M. et al., 2004. The simulation model SCIARA: the 1991 and 2001 lava flows at Mount  
1357 Etna. *Journal of Volcanology and Geothermal Research*, 132(2-3), pp.253–267.
- 1358 Crisp, J.D., 1952. The Use of Gelatin Models in Structural Analysis. *Proceedings of the*



- 1359 Institution of Mechanical Engineers, Part B: Journal of Engineering Manufacture, 1(1-12),  
1360 pp.580–604.
- 1361 Dade, W.B. & Huppert, H.E., 1996. Emplacement of the Taupo ignimbrite by a dilute turbulent  
1362 flow. *Nature*, 381(6582), pp.509–512.
- 1363 Dahm, T., 2000. Numerical simulations of the propagation path and the arrest of fluid-filled  
1364 fractures in the Earth. *Geophysical Journal International*, 141, pp.623–638.
- 1365 Daniels, K.A. & Menand, T., 2015. An experimental investigation of dyke injection under  
1366 regional extensional stress. *Journal of Geophysical Research*, 120(3), pp.2014–2035.
- 1367 Darnell, A.R. et al., 2012. Geographical information system approaches for hazard mapping of  
1368 dilute lahars on Montserrat, West Indies. *Bulletin of volcanology*, 74(6), pp.1337–1353.
- 1369 Daubrée, A., 1891. Recherches expérimentales sur le rôle possible des gaz à hautes  
1370 températures doués de très fortes pressions et animés d'un mouvement fort rapide dans  
1371 divers phénomènes géologiques. *Bulletin de la Société géologique de France*, 19, pp.313–  
1372 354.
- 1373 de Bremond d'Ars, J., Arndt, N.T. & Hallot, E., 2001. Analog experimental insights into the  
1374 formation of magmatic sulfide deposits. *Earth and Planetary Science Letters*, 186,  
1375 pp.371–381.
- 1376 Degruyter, W. & Bonadonna, C., 2013. Impact of wind on the condition for column collapse  
1377 of volcanic plumes. *Earth and Planetary Science Letters*, 377-378, pp.218–226.
- 1378 Del Gaudio, P., Ventura, G. & Taddeucci, J., 2013. The effect of particle size on the rheology  
1379 of liquid-solid mixtures with application to lava flows: Results from analogue  
1380 experiments. *Geochemistry Geophysics Geosystems*, 14(8), pp.2661–2669.
- 1381 Del Bello, E. et al., 2017. Effect of particle volume fraction on the settling velocity of volcanic  
1382 ash particles: insights from joint experimental and numerical simulations. *Scientific  
1383 Reports*, 7, pp.39620.
- 1384 Dellino, P. et al., 2007. Large-scale experiments on the mechanics of pyroclastic flows: Design,  
1385 engineering, and first results. *Journal of Geophysical Research-Solid Earth*, 112(B4).
- 1386 Dellino, P. et al., 2014. Volcanic jets, plumes, and collapsing fountains: evidence from large-  
1387 scale experiments, with particular emphasis on the entrainment rate. *Bulletin of  
1388 volcanology*, 76(834), pp.1–18.
- 1389 de' Michieli Vitturi, M. et al., 2016. Uncertainty quantification and sensitivity analysis of  
1390 volcanic columns models: Results from the integral model PLUME-MoM. *Journal of  
1391 Volcanology and Geothermal Research*, 326, pp.77–91.
- 1392 Di Giuseppe, E. et al., 2009. Gelatins as rock analogs: A systematic study of their rheological  
1393 and physical properties. *Tectonophysics*, 473(3-4), pp.391–403.
- 1394 Di Giuseppe, E. et al., 2015. Characterization of Carbopol® hydrogel rheology for experimental



- 1395 tectonics and geodynamics. *Tectonophysics*, 642(C), pp.29–45.
- 1396 Didden, N. & Maxworthy, T., 1982. The viscous spreading of plane and axisymmetric gravity  
1397 currents. *Journal of Fluid Mechanics*, 121, pp.27–42.
- 1398 Dioguardi, F., Mele, D., Dellino, P. and Dürig, T., 2017. The terminal velocity of volcanic  
1399 particles with shape obtained from 3D X-ray microtomography. *Journal of Volcanology  
1400 and Geothermal Research*, 329, pp.41-53.
- 1401 Doyle, E.E. et al., 2008. Modeling dense pyroclastic basal flows from collapsing columns.  
1402 *Geophysical Research Letters*, 35(4), p.L04305.
- 1403 Dufek, J., 2016. The Fluid Mechanics of Pyroclastic Density Currents. *Annual Review of Fluid  
1404 Mechanics*, 48, pp.459–485.
- 1405 Engwell, S.L. et al., 2016. Insights into the formation and dynamics of coignimbrite plumes  
1406 from one-dimensional models. *Journal of Geophysical Research*, 121, pp.4211–4231.
- 1407 Ernst, G., Davis, J.P. & Sparks, R., 1994. Bifurcation of volcanic plumes in a crosswind. *Bulletin  
1408 of volcanology*, 56, pp.159–169.
- 1409 Esposti Ongaro, T. et al., 2012. Multiphase flow dynamics of pyroclastic density currents  
1410 during the May 18, 1980 lateral blast of Mount St. Helens. *Journal of Geophysical  
1411 Research-Solid Earth*, 117(B06208).
- 1412 Fink, J.H. & Bridges, N.T., 1995. Effects of eruption history and cooling rate on lava dome  
1413 growth. *Bulletin of volcanology*, 57, pp.229–239.
- 1414 Fink, J.H. & Griffiths, R.W., 1990. Radial spreading of viscous-gravity currents with solidifying  
1415 crust. *Journal of Fluid Mechanics*, 221, pp.485–509.
- 1416 Fiske, R.S. & Jackson, E.D., 1972. Orientation and Growth of Hawaiian Volcanic Rifts: The  
1417 Effect of Regional Structure and Gravitational Stresses. *Proceedings of the Royal Society  
1418 A: Mathematical, Physical and Engineering Sciences*, 329(1578), pp.299–326.
- 1419 Folch, A., 2012. A review of tephra transport and dispersal models: Evolution, current status,  
1420 and future perspectives. *Journal of Volcanology and Geothermal Research*, 235-236(C),  
1421 pp.96–115.
- 1422 Folch, A., Costa, A. & Macedonio, G., 2016. FPLUME-1.0: An integral volcanic plume model  
1423 accounting for ash aggregation. *Geoscientific Model Development*, 9(1), pp.431–450.
- 1424 Fukushima, Y., Cayol, V. & Durand, P., 2005. Finding realistic dike models from interferometric  
1425 synthetic aperture radar data: The February 2000 eruption at Piton de la Fournaise.  
1426 *Journal of Geophysical Research*, 110(B03206).
- 1427 Galerne, C.Y. et al., 2011. 3D relationships between sills and their feeders: evidence from the  
1428 Golden Valley Sill Complex (Karoo Basin) and experimental modelling. *Journal of  
1429 Volcanology and Geothermal Research*, 202(3-4), pp.189–199.



- 1430 Galgana, G.A., Grosfils, E.B. & McGovern, P.J., 2013. Radial dike formation on Venus: Insights  
1431 from models of uplift, flexure and magmatism. *Icarus*, 225(1), pp.538–547.
- 1432 Galland, O. et al., 2006. Use of vegetable oil and silica powder for scale modelling of magmatic  
1433 intrusion in a deforming brittle crust. *Earth and Planetary Science Letters*, 243(3-4),  
1434 pp.786–804.
- 1435 Galland, O., 2012. Experimental modelling of ground deformation associated with shallow  
1436 magma intrusions. *Earth and Planetary Science Letters*, 317-318(C), pp.145–156.
- 1437 Galland, O. & Scheibert, J., 2013. Analytical model of surface uplift above axisymmetric flat-  
1438 lying magma intrusions: Implications for sill emplacement and geodesy. *Journal of*  
1439 *Volcanology and Geothermal Research*, 253, pp.114–130.
- 1440 Galland, O. et al., 2014. Dynamics of dikes versus cone sheets in volcanic systems. *Journal of*  
1441 *Geophysical Research*, 10.1002/2014BJ011059.
- 1442 Galland, O. et al., 2015. Laboratory modelling of Volcano Plumbing Systems: A Review. In  
1443 *Advance in Volcanology*. Springer, pp. 1–68.
- 1444 Galland, O., Bertelsen, H.S. & Guldstrand, F., 2016. Application of open-source  
1445 photogrammetric software MicMac for monitoring surface deformation in laboratory  
1446 models. *Journal of Geophysical Research-Solid Earth*, 121, pp.2852–2872.
- 1447 Gilbert, E. & Merle, O., 1987. Extrusion and radial spreading beyond a closing channel. *Journal*  
1448 *of Structural Geology*, 9(4), pp.481–490.
- 1449 Gilbert, J.S. & Sparks, R., 1998. Future research directions on the physics of explosive volcanic  
1450 eruptions. In J. S. Gilbert & R. S. J. Sparks, eds. *The Physics of Explosive Volcanic Eruptions*.  
1451 Geological Society, London, Special Publications, pp. 1–7.
- 1452 Glazner, A.F. et al., 2004. Are plutons assembled over millions of years by amalgamation from  
1453 small magma chambers? *GSA Today*, 14(4), pp.4–11.
- 1454 Goehring, L. & Morris, S.W., 2005. Order and disorder in columnar joints. *Europhysics Letters*,  
1455 69(5), pp.739–745.
- 1456 Goehring, L., Morris, S.W. & Lin, Z., 2006. An Experimental Investigation of the Scaling of  
1457 Columnar Joints. *Physical Review E*, 74(3).
- 1458 Gregg, T. & Fink, J.H., 1995. Quantification of submarine lava-flow morphology through  
1459 analog experiments. *Geology*, 23(1), pp.73–76.
- 1460 Gressier, J.-B. et al., 2010. Control of pore fluid pressure on depth of emplacement of  
1461 magmatic sills: An experimental approach. *Tectonophysics*, 489(1-4), pp.1–13.
- 1462 Griffiths, R.W. & Fink, J.H., 1993. Effects of surface cooling on the spreading of lava flows and  
1463 domes. *Journal of Fluid Mechanics*, 252, pp.667–702.
- 1464 Griffiths, R.W. & Fink, J.H., 1997. Solidifying Bingham extrusions: a model for the growth of



- 1465        silicic lava domes. *Journal of Fluid Mechanics*, 347, pp.13–36.
- 1466        Hall, J., 1805. Experiments on whinstone and lava. *Transactions of the Royal Society of*  
1467        *Edinburgh*, 5(1), pp.43–75.
- 1468        Hall, J., 1815. On the vertical position and convolvement of certain strata, and their relation  
1469        with Granite. *Transactions of the Royal Society of Edinburgh*, 7(1), pp.81–113.
- 1470        Hallworth, M.A., Huppert, H.E. & Sparks, R., 1987. A laboratory simulation of basaltic lava  
1471        flows. *Modern Geology*, 11, pp.93–107.
- 1472        Hamilton, W., & Cadell, T. (1774). Observations on Mount Vesuvius, Mount Etna, and Other  
1473        Volcanoes: In a Series of Letters, Addressed to the Royal Society.
- 1474        Harris, A.J.L., 2008. Modeling lava lake heat loss, rheology, and convection. *Geophysical*  
1475        *Research Letters*, 35(L07303).
- 1476        Herschel, V.W.H. & Bulkley, R., 1926. Konsistenzmessungen von Gummi-Benzollösungen.  
1477        *Kolloid-Zeitschrift*, 39(4), pp.291–300.
- 1478        Herzog, M. & Graf, H.-F., 2010. Applying the three-dimensional model ATHAM to volcanic  
1479        plumes: Dynamic of large co-ignimbrite eruptions and associated injection heights for  
1480        volcanic gases. *Geophysical Research Letters*, 37(L19807).
- 1481        Hickey, J. et al., 2016. Thermomechanical controls on magma supply and volcanic  
1482        deformation: application to Aira caldera, Japan. *Scientific Reports*, 6(32691).
- 1483        Hubbert, M.K., 1937. Theory of scale models as applied to the study of geologic structures.  
1484        *Bulletin of the Geological Society of America*, 48(10), pp.1459–1517.
- 1485        Hubbert, M.K. & Willis, D.G., 1957. Mechanics of hydraulic fracturing, *Petroleum*  
1486        *Transactions, AIME*.
- 1487        Hulme, G., 1974. The interpretation of lava flow morphology. *Geophysical Journal of the Royal*  
1488        *Astronomical Society*, 39, pp.361–383.
- 1489        Huppert, H.E. & Sparks, R., 1985. Komatiites I: Eruption and flow. *Journal of Petrology*.
- 1490        Huppert, H.E. & Sparks, R., 1980. The fluid dynamics of a basaltic magma chamber replenished  
1491        by influx of hot, dense ultrabasic magma. *Contributions to Mineralogy and Petrology*, 75,  
1492        pp.279–289.
- 1493        Huppert, H.E. et al., 1986. A laboratory simulation of pyroclastic flows down slopes. *Journal*  
1494        *of Volcanology and Geothermal Research*, 30, pp.179–199.
- 1495        Huppert, H.E. & Turner, J.S., 1981a. A laboratory model of a replenished magma chamber.  
1496        *Earth and Planetary Science Letters*, 54, pp.144–152.
- 1497        Huppert, H.E. & Turner, J.S., 1981b. Double-diffusive convection. *Journal of Fluid Mechanics*,  
1498        106, pp.299–329.



- 1499 Huppert, H.E. et al., 1986. A laboratory simulation of pyroclastic flows down slopes. *Journal*  
1500 *of Volcanology and Geothermal Research*, 30, pp.179–199.
- 1501 Huppert, H.E., Sparks, R. & Turner, J.S., 1982. Effects of volatiles on mixing in calc-alkaline  
1502 magma systems. *Nature*, 297, pp.554–557.
- 1503 Huppert, H.E., Sparks, R. & Turner, J.S., 1983. Laboratory investigations of viscous effects in  
1504 replenished magma chambers. *Earth and Planetary Science Letters*, 65, pp.377–381.
- 1505 Huppert, H.E. & Hallworth, M.A., 2007. Bi-directional flows in constrained systems. *Journal of*  
1506 *Fluid Mechanics*, 578, pp.95–112.
- 1507 Hutton, J., 1788. *Theory of the Earth; Or an Investigation of the Laws Observable in the*  
1508 *Composition, Dissolution, and Restoration of Land Upon the Globe*. *Transactions of the*  
1509 *Royal Society of Edinburgh*, 1(2), pp.209–304.
- 1510 Hyndman, D.W. & Alt, D., 1987. Radial dikes, laccoliths, and gelatin models. *Journal of*  
1511 *Geology*, 95, pp.763–774.
- 1512 Ishibashi, H., 2009. Non-Newtonian behavior of plagioclase-bearing basaltic magma:  
1513 Subliquidus viscosity measurement of the 1707 basalt of Fuji volcano, Japan. *Journal of*  
1514 *Volcanology and Geothermal Research*, 181(1-2), pp.78–88.
- 1515 Iverson, R.M., 2015. Scaling and design of landslide and debris-flow experiments.  
1516 *Geomorphology*, 244, pp.9–20.
- 1517 Iverson, R.M. et al., 2011. Positive feedback and momentum growth during debris-flow  
1518 entrainment of wet bed sediment. *Nature Geoscience*, 4(2), pp.116–121.
- 1519 Iverson, R.M. et al., 2010. The perfect debris flow? Aggregated results from 28 large-scale  
1520 experiments. *Journal of Geophysical Research*, 115(F3), p.F03005.
- 1521 Ivey, G.N. & Blake, S., 1985. Axisymmetric withdrawal and inflow in a density-stratified  
1522 container. *Journal of Fluid Mechanics*, 161, pp.115–137.
- 1523 Johnson, A.M. & Pollard, D.D., 1973. Mechanics of Growth of Some Laccolithic Intrusions in  
1524 the Henry Mountains, Utah, I. *Tectonophysics*, 18, pp.261–309.
- 1525 Johnson, C.G. et al., 2015. Modelling intrusions through quiescent and moving ambients.  
1526 *Journal of Fluid Mechanics*, 771, pp.370–406.
- 1527 Kaminski, E., Tait, S. & Carazzo, G., 2005. Turbulent entrainment in jets with arbitrary  
1528 buoyancy. *Journal of Fluid Mechanics*, 526, pp.361–376.
- 1529 Karlstrom, L. & Manga, M., 2006. Origins and implications of zigzag rift patterns on lava lakes.  
1530 *Journal of Volcanology and Geothermal Research*, 154(3-4), pp.317–324.
- 1531 Kavanagh, J., Menand, T. & Daniels, K.A., 2013. Gelatine as a crustal analogue: Determining  
1532 elastic properties for modelling magmatic intrusions. *Tectonophysics*, 582, pp.101–111.



- 1533 Kavanagh, J.L. & Dennis, D., 2015. The dynamics of magma ascent in the crust: Characterising  
1534 fluid flow and host-rock deformation using scaled analogue experiments. In EGU General  
1535 Assembly Conference Abstracts. p. 7737.
- 1536 Kavanagh, J.L. & Dennis, D.J.C., 2014. Coupling fluid dynamics and host-rock deformation  
1537 associated with magma intrusion in the crust: Insights from analogue experiments. In  
1538 AGU Fall Meeting Abstracts. p. 4790.
- 1539 Kavanagh, J.L. et al., Controls on sill and dyke-sill hybrid geometry and propagation in the  
1540 crust: The role of fracture toughness. *Tectonophysics*, 698, pp.109-120.
- 1541 Kavanagh, J.L., Boutelier, D. & Cruden, A.R., 2015. The mechanics of sill inception, propagation  
1542 and growth: Experimental evidence for rapid reduction in magmatic overpressure. *Earth  
1543 and Planetary Science Letters*, 421, pp.117-128.
- 1544 Kavanagh, J.L., Menand, T. & Sparks, R.S.J., 2006. An experimental investigation of sill  
1545 formation and propagation in layered elastic media. *Earth and Planetary Science Letters*,  
1546 245(3-4), pp.799-813.
- 1547 Kerr, R.C., 2001. Thermal erosion by laminar lava flows. *Journal of Geophysical Research-Solid  
1548 Earth*, 106, pp.453-465.
- 1549 Kervyn, M. et al., 2010. 3D imaging of volcano gravitational deformation by computerized X-  
1550 ray micro-tomography. *Geosphere*, 6(5), pp.482-498.
- 1551 Kervyn, M. et al., 2009. Volcano load control on dyke propagation and vent distribution:  
1552 Insights from analogue modeling. *Journal of Geophysical Research*, 114(B3), p.B03401.
- 1553 Keszthelyi, L., 1995. A preliminary thermal budget for lava tubes on the Earth and planets.  
1554 *Journal of Geophysical Research-Solid Earth*, 100(B10), pp.20411-20420.
- 1555 Keszthelyi, L. & Denlinger, R., 1996. The initial cooling of pahoehoe flow lobes. *Bulletin of  
1556 volcanology*, 58, pp.5-18.
- 1557 Kotsovinos, N.E., 2000. Axisymmetric submerged intrusion in stratified fluid. *Journal of  
1558 Hydraulic Engineering*, 126(6), pp.446-456.
- 1559 Koyaguchi, T. & Takada, A., 1994. An experimental study on the formation of composite  
1560 intrusions from zoned magma chambers. *Journal of Volcanology and Geothermal  
1561 Research*, 59, pp.261-267.
- 1562 Koyaguchi, T., Ochiai, K. & Suzuki, Y.J., 2009. *Journal of Volcanology and Geothermal  
1563 Research*. *Journal of Volcanology and Geothermal Research*, 186(1-2), pp.68-78.
- 1564 Lane, S.J, et al., 2001. Experimental observations of pressure oscillations and flow regimes in  
1565 an analogue volcanic system. *Journal of Geophysical Research*, 106(B4), pp.6461-6476.
- 1566 Le Corvec, N., Menand, T. & Lindsay, J., 2013. Interaction of ascending magma with pre-  
1567 existing crustal fractures in monogenetic basaltic volcanism: an experimental approach.  
1568 *Journal of Geophysical Research-Solid Earth*, 118(3), pp.968-984.



- 1569 Le Corvec, N. et al., 2015. Effects of crustal-scale mechanical layering on magma chamber  
 1570 failure and magma propagation within the Venusian lithosphere. *Journal of Geophysical*  
 1571 *Research: Planets*, 120, pp.1279–1297.
- 1572 Leitch, A.M., 2004. Analog experiments on melting and contamination at the roof and walls  
 1573 of magma chambers. *Journal of Volcanology and Geothermal Research*, 129(1-3), pp.173–  
 1574 197.
- 1575 Lejeune, A.M. & Richet, P., 1995. Rheology of crystal-bearing silicate melts: An experimental  
 1576 study at high viscosities. *Journal of Geophysical Research-Solid Earth*, 100(B3), pp.4215–  
 1577 4229.
- 1578 Leuthold, J. et al., 2012. Time resolved construction of a bimodal laccolith (Torres del Paine,  
 1579 Patagonia). *Earth and Planetary Science Letters*, 325-326, pp.85–92.
- 1580 Lister, J.R., 1990. Buoyancy-driven fluid fracture: the effects of material toughness and of low-  
 1581 viscosity precursors. *Journal of Fluid Mechanics*, 210, pp.263–280.
- 1582 Llewellyn, E., Mader, H. & Wilson, S., 2002a. The constitutive equation and flow dynamics of  
 1583 bubbly magmas. *Geophysical Research Letters*, 29(24).
- 1584 Llewellyn, E., Mader, H. & Wilson, S., 2002b. The rheology of a bubbly liquid. *Proceedings of*  
 1585 *the Royal Society A: Mathematical, Physical and Engineering Sciences*, 458(2020),  
 1586 pp.987–1016.
- 1587 Loughlin, S.C. et al. eds., 2015. *Global Volcanic Hazards and Risk*, Cambridge, UK: Cambridge  
 1588 University Press, pp.393.
- 1589 Lube, G. et al., 2015. Synthesizing large-scale pyroclastic flows: Experimental design, scaling,  
 1590 and first results from PELE. *Journal of Geophysical Research-Solid Earth*, 120(3).
- 1591 Lundstrom, C.C. & Glazner, A.F., 2016. Silicic Magmatism and the Volcanic–Plutonic  
 1592 Connection. *Elements*, 12(2), pp.91–96.
- 1593 Lyman, A.W., Koenig, E. & Fink, J.H., 2004. Predicting yield strengths and effusion rates of lava  
 1594 domes from morphology and underlying topography. *Journal of Volcanology and*  
 1595 *Geothermal Research*, 129(1-3), pp.125–138.
- 1596 Maccaferri, F., Bonafede, M. & Rivalta, E., 2011. A quantitative study of the mechanisms  
 1597 governing dike propagation, dike arrest and sill formation. *Journal of Volcanology and*  
 1598 *Geothermal Research*, 208(3), pp.39–50.
- 1599 Mader, H.M., Llewellyn, E.W. & Mueller, S.P., 2013. *Journal of Volcanology and Geothermal*  
 1600 *Research*. *Journal of Volcanology and Geothermal Research*, 257(C), pp.135–158.
- 1601 Mader, H.M., Manga, M. & Koyaguchi, T., 2004. The role of laboratory experiments in  
 1602 volcanology. *Journal of Volcanology and Geothermal Research*, 129(1-3), pp.1–5.
- 1603 Manga, M. & Loewenberg, M., 2001. Viscosity of magmas containing highly deformable  
 1604 bubbles. *Journal of Volcanology and Geothermal Research*, 105, pp.19–24.



- 1605 Manga, M. et al., 1998. Rheology of bubble-bearing magmas. *Journal of Volcanology and*  
1606 *Geothermal Research*, 87, pp.15–28.
- 1607 Manville, V., Major, J.J. & Fagents, S.A., 2013. Modeling lahar behavior and hazards. In S. A.  
1608 Fagents, T. K. P. Gregg, & R. M. C. Lopes, eds. *Modeling Volcanic Processes: The Physics*  
1609 *and Mathematics of Volcanism*. Cambridge University Press, pp. 300–330.
- 1610 Manzella, I. et al., 2015. The role of gravitational instabilities in deposition of volcanic ash.  
1611 *Geology*, 43(3), pp.211–214.
- 1612 Mathieu, L. et al., 2008. Dykes, cups, saucers and sills: Analogue experiments on magma  
1613 intrusion into brittle rocks. *Earth and Planetary Science Letters*, 271(1-4), pp.1–13.
- 1614 Mazzarini, F. et al., 2010. Relations between deformation and upper crustal magma  
1615 emplacement in laboratory physical models. *Tectonophysics*, 484(1-4), pp.139–146.
- 1616 McGuire, W.J. & Pullen, A.D., 1989. Location and orientation of eruptive fissures and feeder  
1617 dykes at Mount Etna; influence of gravitational and regional tectonic stress regimes.  
1618 *Journal of Volcanology and Geothermal Research*, 38(3-4), pp.325–344.
- 1619 McLeod, P. & Tait, S., 1999. The growth of dykes from magma chambers. *Journal of*  
1620 *Volcanology and Geothermal Research*, 92(3-4), pp.231–245.
- 1621 Menand, T. & Tait, S.R., 2001. A phenomenological model for precursor volcanic eruptions.  
1622 *Nature*, 411, pp.678–680.
- 1623 Menand, T. & Tait, S.R., 2002. The propagation of a buoyant liquid-filled fissure from a source  
1624 under constant pressure: An experimental approach. *Journal of Geophysical Research*,  
1625 107(2306), pp.177–185.
- 1626 Menand, T., Daniels, K.A. & Benghiat, P., 2010. Dyke propagation and sill formation in a  
1627 compressive tectonic environment. *Journal of Geophysical Research*, 115(B08201),  
1628 pp.doi:10.1029/2009JB006791.
- 1629 Merle, O., 2015. The scaling of experiments on volcanic systems. *Frontiers in Earth Science*, 3,  
1630 Article 26.
- 1631 Michaut, C., 2011. Dynamics of magmatic intrusions in the upper crust: Theory and  
1632 applications to laccoliths on Earth and the Moon. *Journal of Geophysical Research*,  
1633 116(B05205).
- 1634 Miyamoto, H. & Sasaki, S., 1997. Simulating lava flows by an improved cellular automata  
1635 method. *Computers and Geosciences*, 23(3), pp.293–292.
- 1636 Miyamoto, H. et al., 2001. Experimental Studies on Non-Newtonian Fluid Flows as Analogues  
1637 of Lava Flows: Toward a Numerical Model with a Cooling Crust. *Theoretical and Applied*  
1638 *Mechanics*, 50(3), pp.283–292.
- 1639 Morton, B.R., Taylor, G. & Turner, J.S., 1956. Turbulent gravitational convection from  
1640 maintained and instantaneous sources. *Proceedings of the Royal Society of London*.



- 1641 Series A, Mathematical and Physical Sciences, 234(1196), pp.1–23.
- 1642 Mueller, S., Llewellyn, E.W. & Mader, H.M., 2011. The effect of particle shape on suspension  
1643 viscosity and implications for magmatic flows. *Geophysical Research Letters*, 38(13).
- 1644 Mueller, S., Llewellyn, E.W. & Mader, H.M., 2009. The rheology of suspensions of solid  
1645 particles. *Proceedings of the Royal Society A: Mathematical, Physical and Engineering*  
1646 *Sciences*, 102, pp.161–179.
- 1647 Mueller, S.B. et al., 2016. Experimental volcanic ash aggregation: Internal structuring of  
1648 accretionary lapilli and the role of liquid bonding. *Earth and Planetary Science Letters*,  
1649 433, pp.232–240.
- 1650 Müller, G., 1998. Starch columns: Analog model for basalt columns. *Journal of Geophysical*  
1651 *Research-Solid Earth*, 103(B7), pp.15239–15253.
- 1652 Muller, J.R., Ito, G. & Martel, S.J., 2001. Effects of volcano loading on dike propagation in an  
1653 elastic half-space. *Journal of Geophysical Research-Solid Earth*, 106(B6), pp.11101–  
1654 11113.
- 1655 Namiki, A. et al., 2016. Sloshing of a bubbly magma reservoir as a mechanism of triggered  
1656 eruptions. *Journal of Volcanology and Geothermal Research*, 320, pp.156–171.
- 1657 Neri, A. & Dobran, F., 1994. Influence of eruption parameters on the thermofluid dynamics of  
1658 collapsing volcanic columns. *Journal of Geophysical Research-Solid Earth*, 99, pp.11833–  
1659 11857.
- 1660 Nolan, M., 2014. Levee stability and the evolution of “A” a lava flow-fields. University of  
1661 Portsmouth.
- 1662 Oppenheimer, J. et al., 2015. Gas migration regimes and outgassing in particle-rich  
1663 suspensions. *Frontiers in Physics*, 3, p.664.
- 1664 Orr, T.R. & Rea, J.C., 2012. Time-lapse camera observations of gas piston activity at Pu’u ‘Ō’ō,  
1665 Kīlauea volcano, Hawai’i. *Bulletin of volcanology*, 74(10), pp.2353–2362.
- 1666 Phillips, J.C. & Woods, A.W., 2001. Bubble plumes generated during recharge of basaltic  
1667 magma reservoirs. *Earth and Planetary Science Letters*, 186, pp.297–309.
- 1668 Pitman, E.B. et al., 2003. Computing granular avalanches and landslides. *Physics of Fluids*,  
1669 15(12), pp.3638–3646.
- 1670 Pollard, D.D., 1973. Derivation and evaluation of a mechanical model for sheet intrusions.  
1671 *Tectonophysics*, 19(3), pp.233–269.
- 1672 Pollard, D.D. & Johnson, A.M., 1973. Mechanics of growth of some laccolithic intrusions in the  
1673 Henry mountains, Utah, II: Bending and failure of overburden layers and sill formation.  
1674 *Tectonophysics*, 18(3-4), pp.311–354.
- 1675 Quareni, F., Tallarico, A. & Dragoni, M., 2004. Modeling of the steady-state temperature field



- 1676 in lava flow levées. *Journal of Volcanology and Geothermal Research*, 132(2-3), pp.241–  
 1677 251.
- 1678 Ramberg, H., 1967. Gravity, Deformation and the Earth's Crust as studied by centrifuged  
 1679 models, Academic Press Inc. London, pp.214.
- 1680 Ramberg, H., 1970. Model studies in relation to intrusion of plutonic bodies. In G. Newall &  
 1681 N. Rast, eds. Mechanism of igneous intrusion. Gallery Press Liverpool, pp. 261–288.
- 1682 Richter, D.H. et al., 1970. Chronological narrative of the 1959-60 eruption of Kilauea volcano,  
 1683 Hawaii. Geological Society Professional Paper 537-E. United States Government Printing  
 1684 Office, Washington, pp.75.
- 1685 Rivalta, E. et al., 2015. A review of mechanical models of dike propagation: Schools of thought,  
 1686 results and future directions. *Tectonophysics*, 638, pp.1–42.
- 1687 Rivalta, E., Böttlinger, M. & Dahm, T., 2005. Buoyancy-driven fracture ascent: Experiments in  
 1688 layered gelatine. *Journal of Volcanology and Geothermal Research*, 144(1-4), pp.273–  
 1689 285.
- 1690 Robertson, J.C. and Kerr, R.C., 2012. Isothermal dynamics of channeled viscoplastic lava flows  
 1691 and new methods for estimating lava rheology. *Journal of Geophysical Research: Solid  
 1692 Earth*, 117(B1).
- 1693 Roche, O., 2012. Depositional processes and gas pore pressure in pyroclastic flows: an  
 1694 experimental perspective. *Bulletin of volcanology*, 74(8), pp.1807–1820.
- 1695 Roman-Berdiel, T., 1999. Geometry of granite emplacement in the upper crust: contributions  
 1696 of analogue modelling. In A. Castro, C. Fernandez, & J. L. Vigneresse, eds. Understanding  
 1697 Granites: Integrating New and Classical Techniques. Geological Society, pp. 77–94.
- 1698 Roman-Berdiel, T., Gapais, D. & Brun, J.P., 1995. Analogue models of laccolith formation.  
 1699 *Journal of Structural Geology*, 17(9), pp.1337–1346.
- 1700 Roman-Berdiel, T., Gapais, D. & Brun, J.P., 1997. Granite intrusion along strike-slip zones in  
 1701 experiment and nature. *American Journal of Science*, 297, pp.651–678.
- 1702 Rongo, R. et al., 2016. SCIARA: cellular automata lava flow modelling and applications in  
 1703 hazard prediction and mitigation. Geological Society London Special Publications, 426(1),  
 1704 pp.345–356.
- 1705 Rossetti, F., Ranalli, G. & Faccenna, C., 1999. Rheological properties of paraffin as an analogue  
 1706 material for viscous crustal deformation. *Journal of Structural Geology*, 21(4), pp.413–  
 1707 417.
- 1708 Rowley, P.J. et al., 2014. Experimental study of dense pyroclastic density currents using  
 1709 sustained, gas-fluidized granular flows. *Bulletin of volcanology*, 76(9):855.
- 1710 Rust, A.C. & Manga, M., 2002a. Bubble Shapes and Orientations in Low Re Simple Shear Flow.  
 1711 *Journal of Colloid and Interface Science*, 249(2), pp.476–480.



- 1712 Rust, A.C. & Manga, M., 2002. Effects of bubble deformation on the viscosity of dilute  
1713 suspensions. *Journal of Non-Newtonian Fluid Mechanics*, 104, pp.53–63.
- 1714 Ruzicka, B. & Zaccarelli, E., 2011. A fresh look at the Laponite phase diagram. *Soft Matter*,  
1715 7(4), pp.1268–1286.
- 1716 Savitski, A.A. & Detournay, E., 2002. Propagation of a penny-shaped fluid-driven fracture in  
1717 an impermeable rock: asymptotic solutions. *International journal of solids and structures*,  
1718 39, pp.6311–6337.
- 1719 Saumur, B.M., Cruden, A.R. & Boutelier, D., 2016. Sulfide Liquid Entrainment by Silicate  
1720 Magma: Implications for the Dynamics and Petrogenesis of Magmatic Sulfide Deposits.  
1721 *Journal of Petrology*, 56(12), pp.2473–2490.
- 1722 Schellart, W.P., 2011. Rheology and density of glucose syrup and honey: Determining their  
1723 suitability for usage in analogue and fluid dynamic models of geological processes. *Journal*  
1724 *of Structural Geology*, 33(6), pp.1079–1088.
- 1725 Scheibert, J., Galland, O. & Hafver, A., 2017. Inelastic deformation during sill and laccolith  
1726 emplacement: insights from an analytic elasto-plastic model. *Journal of Geophysical*  
1727 *Research*, 121, doi: 10.1002/2016JB013754.
- 1728 Schilling, S.P., 2014. Laharz\_py: GIS tools for automated mapping of lahar inundation hazard  
1729 zones, U.S. Geological Survey Report 1073.
- 1730 Schreurs, G. et al., 2006. Analogue benchmarks of shortening and extension experiments. In  
1731 S. Buitter & G. Schreurs, eds. *Analogue and numerical modelling of crustal-scale processes*.  
1732 Geological Society, London, Special Publications, pp. 1–27.
- 1733 Scollo, S. et al., 2008. Sensitivity analysis and uncertainty estimation for tephra dispersal  
1734 models. *Journal of Geophysical Research*, 113(B6), p.B06202.
- 1735 Sheets, P., 2015. Volcanoes, Ancient People, and their Societies. In H. Sigurdsson et al., eds.  
1736 *The Encyclopedia of Volcanoes*. Elsevier, pp. 1313–1319.
- 1737 Sigurdsson, H., 2015. The History of Volcanology. In H. Sigurdsson et al., eds. *The Encyclopedia*  
1738 *of Volcanoes*. Elsevier, pp. 13–32.
- 1739 Sigurdsson, H., 2015b. Volcanoes in Art. In H. Sigurdsson et al., eds. *The Encyclopedia of*  
1740 *Volcanoes*. Elsevier, pp. 1321–1343.
- 1741 Soule, S.A. & Cashman, K.V., 2005. Shear rate dependence of the pāhoehoe-to-‘a‘ā transition:  
1742 Analog experiments. *Geology*, 33(5), p.361.
- 1743 Sparks, R., 1986. The dimensions and dynamics of volcanic eruption columns. *Bulletin of*  
1744 *volcanology*, 48, pp.3–15.
- 1745 Sparks, R. & Wilson, L., 1976. A model for the formation of ignimbrite by gravitational column  
1746 collapse. *Journal of the Geological Society*, 132, pp.441–451.



- 1747 Sparks, R. et al., 1993. Sediment-laden gravity currents with reversing buoyancy. *Earth and*  
1748 *Planetary Science Letters*, 114, pp.243–257.
- 1749 Sparks, R.S.J., 2009. The legacy of George Walker to volcanology. In *Studies in Volcanology:*  
1750 *The legacy of George Walker*. The Geological Society of London, pp. 1–16.
- 1751 Sparks, R. & Cashman, K.V., 2017. Dynamic Magma Systems: Implications for Forecasting  
1752 Volcanic Activity. *Elements*.
- 1753 Spence, D.A., Sharp, P.W. & Turcotte, D.L., 1987. Buoyancy-driven crack propagation: a  
1754 mechanism for magma migration. *Journal of Fluid Mechanics*, 174, pp.135–153.
- 1755 Stasiuk, M.V. et al., 1993. Influence of cooling on lava-flow dynamics. *Geology*, 21(4), pp.335–  
1756 338.
- 1757 Sulpizio, R. & Pierfrancesco D., 2008. Sedimentology, depositional mechanisms and pulsating  
1758 behaviour of pyroclastic density currents. In: *Developments in Volcanology 10*, p.57-96.
- 1759 Suzuki, Y.J. & Koyaguchi, T., 2012. 3-D numerical simulations of eruption column collapse:  
1760 Effects of vent size on pressure-balanced jet/plumes. *Journal of Volcanology and*  
1761 *Geothermal Research*, 221-222, pp.1–13.
- 1762 Suzuki, Y.J. & Koyaguchi, T., 2009. A three-dimensional numerical simulation of spreading  
1763 umbrella clouds. *Journal of Geophysical Research*, 114(B3), p.B03209.
- 1764 Suzuki, Y.J. & Koyaguchi, T., 2015. Effects of wind on entrainment efficiency in volcanic  
1765 plumes. *Journal of Geophysical Research-Solid Earth*, 120, pp.6122–6140.
- 1766 Svensen, H. et al., 2004. Release of methane from a volcanic basin as a mechanism for initial  
1767 Eocene global warming. *Nature*, 429(6991), pp.542–245.
- 1768 Taisne, B. & Tait, S., 2011. Effect of solidification on a propagating dike. *Journal of Geophysical*  
1769 *Research*, 116(B1), p.B01206.
- 1770 Taisne, B., Tait, S. & Jaupart, C., 2011. Conditions for the arrest of a vertical propagating dyke.  
1771 *Bulletin of volcanology*, 73(2), pp.191–204.
- 1772 Takada, A., 1990. Experimental study on propagation of liquid-filled crack in gelatin: shape  
1773 and velocity in hydrostatic stress condition. *Journal of Geophysical Research*, 95,  
1774 pp.8471–8481.
- 1775 Truby, J.M. et al., 2015. The rheology of three-phase suspensions at low bubble capillary  
1776 number. *Proceedings of the Royal Society A: Mathematical, Physical and Engineering*  
1777 *Sciences*, 471(2173), p.20140557.
- 1778 Turner, J.S., Huppert, H.E. & Sparks, R., 1983. An experimental investigation of volatile  
1779 exsolution in evolving magma chambers. *Journal of Volcanology and Geothermal*  
1780 *Research*, 16, pp.263–277.
- 1781 Valentine, G.A. et al., 2015. Experiments with vertically and laterally migrating subsurface



- 1782 explosions with applications to the geology of phreatomagmatic and hydrothermal  
 1783 explosion craters and diatremes. *Bulletin of volcanology*, 77(15), pp.1–17.
- 1784 Valentine, G.A., Wohletz, K.H. & Kieffer, S.W., 1992. Effects of topography on facies and  
 1785 compositional zonation in caldera-related ignimbrites. *Geological Society of America*  
 1786 *Bulletin*, 104, pp.154–165.
- 1787 van Otterloo, J. & Cruden, A.R., 2016. Rheology of pig skin gelatine: Defining the elastic  
 1788 domain and its thermal and mechanical properties for geological analogue experiment  
 1789 applications. *Tectonophysics*, 683, pp.86–97.
- 1790 Vicari, A. et al., 2007. Modeling of the 2001 lava flow at Etna volcano by a Cellular Automata  
 1791 approach. *Environmental Modelling & Software*, 22(10), pp.1465–1471.
- 1792 Walker, G., 1967. Thickness and viscosity of Etnean lavas. *Nature*, pp.484–485.
- 1793 Walker, G., 1960. Zeolite zones and dike distribution in relation to the structure of the basalts  
 1794 of eastern Iceland. *The Journal of Geology*, 68(5), pp.515–528.
- 1795 Walker, G., Wilson, L. & Bowell, E.L.G., 1971. Explosive Volcanic Eruptions—I The Rate of Fall  
 1796 of Pyroclasts. *Geophysical Journal of the Royal Astronomical Society*, 22(4).
- 1797 Walter, T.R. & Troll, V.R., 2003. Experiments on rift zone evolution in unstable volcanic  
 1798 edifices. *Journal of Volcanology and Geothermal Research*, 127(1-2), pp.107–120.
- 1799 Watanabe, T. et al., 2002. Analogue experiments on magma-filled cracks: competition  
 1800 between external stresses and internal pressure. *Earth Planets and Space*, 54, pp.1247–  
 1801 1261.
- 1802 Weertman, J., 1971. Theory of water-filled crevasses in glaciers applied to vertical magma  
 1803 transport beneath oceanic ridges. *Journal of Geophysical Research*, 76(5), pp.1171–1183.
- 1804 Weinberg, R.F. & Leitch, A.M., 1998. Mingling in mafic magma chambers replenished by light  
 1805 felsic inputs: fluid dynamical experiments. *Earth and Planetary Science Letters*, 157,  
 1806 pp.41–56.
- 1807 Williams, R., Stinton, A.J. & Sheridan, M.F., 2008. *Journal of Volcanology and Geothermal*  
 1808 *Research*. *Journal of Volcanology and Geothermal Research*, 177(4), pp.762–768.
- 1809 Wilson, L. & Walker, G., 1987. Explosive volcanic eruptions-VI. Ejecta dispersal in plinian  
 1810 eruptions: the control of eruption conditions and atmospheric properties. *Geophysical*  
 1811 *Journal of the Royal Astronomical Society*, 89, pp.657–679.
- 1812 Wilson, L. et al., 1978. The control of volcanic column heights by eruption energetics and  
 1813 dynamics. *Journal of Geophysical Research*, 83(B4), pp.1829–1836.
- 1814 Witham, F., Woods, A.W. & Gladstone, C., 2006. An analogue experimental model of depth  
 1815 fluctuations in lava lakes. *Bulletin of volcanology*, 69(1), pp.51–56.
- 1816 Woodhouse, M.J. et al., 2013. Interaction between volcanic plumes and wind during the 2010



- 1817 Eyjafjallajökull eruption, Iceland. *Journal of Geophysical Research-Solid Earth*, 118(1),  
1818 pp.92–109.
- 1819 Woods, A.W., 1988. The fluid dynamics and thermodynamics of eruption columns. *Bulletin of*  
1820 *volcanology*, 50, pp.169–193.
- 1821 Woods, A.W. & Bursik, M.I., 1994. A laboratory study of ash flows. *Journal of Geophysical*  
1822 *Research-Solid Earth*, 99(B3), pp.4375–4394.
- 1823 Woods, A.W. & Caulfield, C., 1992. A laboratory study of explosive volcanic eruptions. *Journal*  
1824 *of Geophysical Research*, 97(B5), pp.6699–6712.
- 1825 Woods, A.W. & Caulfield, C.P., 2007. A laboratory study of explosive volcanic eruptions.  
1826 *Journal of Geophysical Research*, 97(B5), pp.6699–6712.
- 1827 Závada, P. et al., 2009. Internal fabric development in complex lava domes. *Tectonophysics*,  
1828 466(1-2), pp.101–113.



1829 **Tables and Captions**

1830 **Table 1.** Properties of analogue materials used to model magmas and lavas for rheology and processes. \*Material not currently used in  
 1831 analogue modeling of volcanic processes however displays properties that may lead to its future use.  
 1832

System Component	Material	Key Properties		Example reference
		Rheology or Mechanical Behaviour	e.g. Viscosity, density, strength	
<i>Magma or Lava analogues</i>				
Syrups	Corn syrup	Newtonian	180 Pa s at 22 °C	Rust and Manga (2002b)
	Glucose syrup	T-dependant Newtonian	454.7 Pa s at 20 °C	Schellart (2011)
Oils	Golden Syrup	Newtonian	50-78 Pa s at 20 °C	Castruccio et al. (2010)
	Honey	Newtonian	200 Pa s at 22 °C	Mathieu et al. (2008)
	Glycerine	Newtonian	Density of 1.26 g cm <sup>3</sup> viscosity of 7.7 cm s <sup>-1</sup>	Huppert and Hallworth (2007)
	Silicon oil	Newtonian	41.32 Pa s at 25 °C	Mueller et al. (2009)
Waxes	Vegetable oil (Vegetaline)	Newtonian	2 x 10 <sup>-2</sup> Pa s at 50 °C	Galland et al. (2006)
	Paraffin	T-dependant Newtonian	10 Pa s at 52 °C	Rossetti et al. (1999)
Other	Polyethylene glycol (PEG)	T-dependant Newtonian	0.18 Pa s at 21 °C	Griffiths and Fink (1997)
	Air	Gas		
	Water	Newtonian	Density of 0.9982 g cm <sup>3</sup> and viscosity of 0.01 cm s <sup>-1</sup> at 20 °C	Huppert and Hallworth (2007)
	RTV silicone	Newtonian	When freshly exposed to air 25 Pa s solidifying after c. 5 hours	Gressier et al. (2010)
	Silicone putty	Viscoelastic/Newtonian	Density of 1.12-1.14 g/cm <sup>3</sup> . Viscosities of 2-2.57 x 10 <sup>4</sup> Pa s at 24 °C	Ramberg (1970)
	Gum rosin with 21.8% acetone	Newtonian	1.07 Pa s at room temperature	Lane et al. (2001)
	Hair gel	Shear thinning	27 Pa s at room temperature	Castruccio et al. (2014)
Shaving foam	Viscoelastic	172 Pa s at room temperature	Bagdassarov and Pinkerton (2004)	



	Collophony and ethyl phthalate mixtures	Viscoelastic	$5.73 \times 10^6$ Pa s at 22 °C. Collophony mixtures are almost Newtonian at low stress	Ramberg (1970)
	Plaster of Paris and water suspensions (2.2 to 2.6 ratio)	Shear thinning	Viscosity of 0.8 - 6.2 Pa s shear rate dependant	Závada et al. (2009)
<b>Host rock analogues</b>				
<b>Gels</b>	Gelatine (pig-skin type)	Viscoelastic	For 2.5 wt% at 10 °C: viscoelastic at strain rates $<0.147$ s <sup>-1</sup> ; however highly variable with different concentrations and temperatures. At strain rate of 10 <sup>-2</sup> s <sup>-1</sup> viscosity is ~50 Pa s.	Di Guiseppe et al. (2009)
	Laponite powder (synthetic clay)*	Viscoelastic	Commonly used as a rheology-modifier with variable behaviour depending on concentration.	Ruzicka and Zaccarelli (2011)
	Carbopol*	Visco-elasto-plastic	Highly variable depending on concentration, shear stress and strain rate	Di Guiseppe et al. (2015)
	Silica flour (spheres and crystals)	Brittle	When compacted: crystals have density of $1.33$ g cm <sup>-3</sup> $\pm$ 0.2%, cohesion of 288 Pa $\pm$ 26 with angle of internal friction 40°. spheres have density of $1.56$ g cm <sup>-3</sup> $\pm$ 0.18%, cohesion of 288 Pa $\pm$ 26 with angle of internal friction ~24°.	Galland et al. (2006)
	Diatomite powder	Frictional	When compacted: density of 400 kg m <sup>-3</sup> cohesion of 300 Pa at normal stresses 50-300 Pa.	Gressier et al. (2010)
<b>Other</b>	Sand	Shear	Cohesion of 0 - 10 Pa, angle of internal friction of 30°	Mathieu et al. (2008)
	Ignimbrite powder (Grande Nape Ignimbrite, Mont Dore volcano, France)	Shear	Cohesion of 100 - 230 Pa, angle of internal friction of 38°	Mathieu et al. (2008)
	Modelling clay	Plastic	At density of $1.71$ g cm <sup>-3</sup> , yield strength $4 \times 10^5$ Pa s. Above yield strength viscosities range from $0.5-7.4 \times 10^7$ Pa s	Ramberg (1970)



Painter's putty	Plastic	Densities of 1.8 to 1.9 g cm <sup>-3</sup> , yield strength of 3 x 10 <sup>3</sup> Pa s. Above yield stress viscosities from 1 x 10 <sup>4</sup> to 10 <sup>7</sup> Pa s	Ramberg (1970)
<b>Particle analogues</b>			
Sand and gravel		Without mud – bulk density of 1710 ± 119 kg m <sup>-3</sup> and internal angle of friction 39° With mud – bulk density of 1650 ± 107 kg m <sup>-3</sup> and internal angle of friction 39°	Iverson et al. (2010)
Spherical glass beads		Density of 2500 kg m <sup>-3</sup>	Mueller et al. (2016)



**Table 2.** Examples of different analogue materials and their combinations used to model different parts of the volcanic and magmatic system.

Processes considered	Analogue Material Combinations			Example studies
	Magma or Lava	Host	Particulates	
<b>Magma</b>				
<i>Two phase: melt + bubbles</i>	Golden syrup with nitrogen	-	-	Llewelin et al. (2002b)
	Aerated golden syrup	-	-	Bagdassarov and Pinkerton (2004)
	Corn syrup with air	-	-	Rust and Manga (2002a, 2002b)
<i>Two phase: melt + crystals</i>	Silicone oil with silica-glass beads	-	-	Mueller et al. (2009), Cimarelli et al. (2011)
	Silicone oil with art glitter	-	-	Mueller et al. (2009)
	Silicone oil with silicon carbide grit	-	-	Mueller et al. (2009), Cimarelli et al. (2011)
	Silicone oil with wollastonite particles	-	-	Mueller et al. (2009), Cimarelli et al. (2011)
	Golden syrup with glass beads	-	-	Mueller et al. (2011)
	Golden syrup with art glitter	-	-	Mueller et al. (2011)
<i>Three phase: melt + bubbles + crystals</i>	Golden syrup with glass fibres	-	-	Mueller et al. (2011)
	Shell Motor oil with paraplex plastic	-	-	Bhattacharji and Smith (1964)
	Epoxy resin with glass beads/carbon fibres	-	-	Cimarelli et al. (2011)
<b>Intrusions</b>	Golden syrup, with air and glass beads	-	-	Truby et al. (2015)



Dykes	Air	Gelatine	-	Muller et al. (2001), Rivalta et al. (2005), Le Corvec et al. (2013)
	Water	Gelatine	-	Fiske and Jackson (1972), McLeod and Tait (1999), Taisne et al. (2011)
	Air and water	Gelatine	-	Menand and Tait (2001)
	Hydroxyethyl cellulose	Gelatine	-	McLeod and Tait (1999)
	Silicone oil	Gelatine	-	McLeod and Tait (1999), Watanabe et al. (2002)
	Golden syrup	Sand and plaster powder mix	-	Kervyn et al. (2009)
	Golden syrup	Gelatine with a sand and plaster mix load	-	Kervyn et al. (2009)
	Golden syrup	Silica flour	-	Abdelmalak et al. (2012)
	Honey	Sand	-	Mathieu et al. (2008)
	Golden syrup	Ignimbrite powder	-	Mathieu et al. (2008)
	Water	Gelatine	-	Kavanagh et al. (2006), Kavanagh et al. (2015)
	Vegetable oil (Vegetaline)	Silica flour	-	Galland et al. (2006; 2012)
	Vegetable oil (Vegetaline)	Gelatine	-	Daniels and Menand (2015), Chanceaux and Menand (2014, 2016)
	RTV silicone	Diatomite powder	-	Gressier et al. (2010)
Larger igneous bodies	Hot salty water injected into cold fresh water	-	-	Huppert et al. (1986)
	$KNO_3$ , $NaNO_3$ and $K_2CO_3$	-	-	Huppert and Turner (1981a), Turner et al. (1983)
	Glycerine-ethanol mix injected into molten PEG 600 wax	-	-	Weinberg and Leitch (1998)
	Hydroxyethylcellulose polymer and silicone oil	-	-	De Bremond d-Ars et al. (2001)
	Diluted glucose syrup and bubbles	-	-	Namiki et al. (2016)
	Water or hydroxyethyl cellulose or silicone oil	Gelatine	-	McLeod and Tait (1999)
Sills				



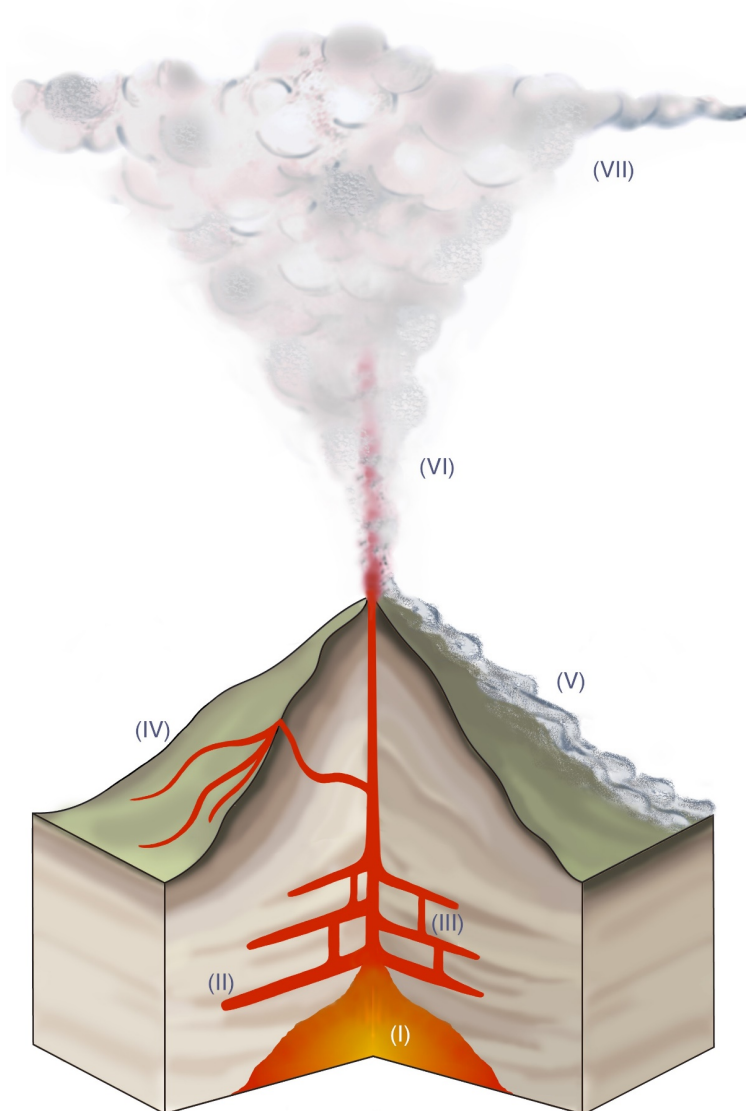
	Sunflower oil/silicone oil and natrosol solution/glucose solution/ Na polytungstate	-	-	Saumur et al. (2016)
	Glycerine	Gelatine	-	Koyaguchi and Takada (1994)
	Grease	Gelatine	-	Pollard and Johnson (1973)
	Silicone putty	Sand layers	-	Roman-Berdiel et al. (1995)
	Silicone putty/KMnO <sub>4</sub> solutions	Modelling clay/painter's putty/Concrete	-	Ramberg (1970)
<b>Lavas</b>				
<i>Lava lakes and hot conduit</i>	Golden syrup mixed with water	-	-	Beckett et al. (2011)
	Water and air	-	-	Witham et al. (2006)
	Paraffin wax	-	-	Karlstrom and Manga (2006)
<i>Lava domes</i>	PEG wax into sucrose solution	-	-	Griffiths and Fink (1993), Fink and Bridges (1995)
	PEG wax with kaolin powder	-	-	Griffiths and Fink (1997), Lyman et al. (2004)
<i>Lava flows</i>	Plaster of Paris seeded with magnetite particles	Sand	-	Závada et al. (2009)
	PEG wax into sucrose solution	-	-	Hallworth et al. (1987), Fink and Griffiths (1990)
	Glucose syrup into sucrose solution	-	-	Stasiuk et al. (1993)
	PEG 600 wax	Peg 600 wax surface	-	Kerr (2001)
	Paraffin wax	-	-	Miyamoto et al. (2001), Nolan (2014)
	Golden syrup and sugar crystals	-	-	Castruccio et al. (2010)
	Hot water	PEG 1000 wax surface	-	Huppert and Sparks (1985)
KNO <sub>3</sub> , NaNO <sub>3</sub> and K <sub>2</sub> CO <sub>3</sub>	-	-	Turner et al. (1983)	
Viscous silicone	-	-	Gilbert and Merle (1987)	
Corn starch and water slurry	-	-	Goehring and Morris (2005),	



					Goehring et al. (2006)
<b>Granular flows</b>					
<i>Pyroclastic density currents</i>	-		-	Particle bearing freshwater injected into saline water	Carey et al. (1988)
	-		-	Methanol-ethylene glycol injected into water	Woods and Bursik (1994)
<i>Lahars</i>	-		-	Sand and gravel with and without mud	Iverson et al. (2010)
<b>Plumes</b>					
<i>Plumes</i>	-		-	Particle bearing freshwater into saline water	Carey et al. (1988)
	-		-	Cold or warm water into cold flowing water	Ernst et al. 1994
<i>Ash dispersal</i>	-		-	Methanol-ethylene glycol injected into fresh water	Woods and Caulfield (1992)
	-		-	Spherical glass beads in water with various additives	Koyaguchi et al. (2009)
<i>Air fall</i>	-		-	Spherical glass beads in water with various additives	Koyaguchi et al. (2009)
	-		-	Soda-lime glass beads suspended in hot air	Mueller et al. (2016)



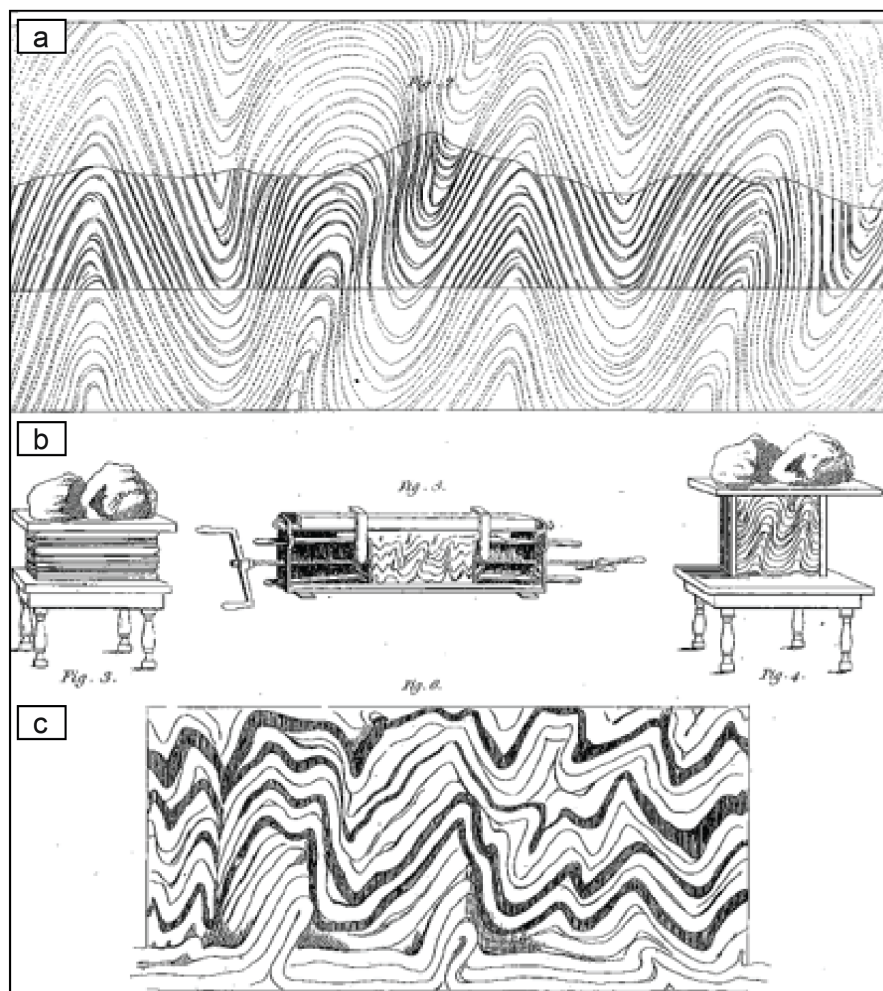
1837 **Figures and captions**



1838

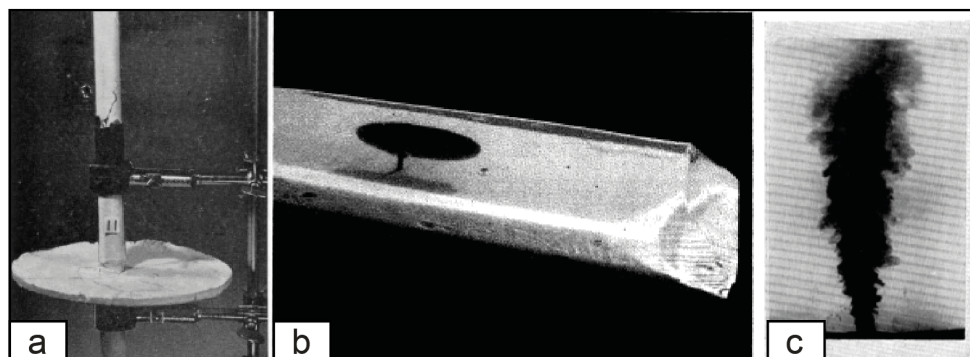
1839 **Figure 1:** Schematic illustration of the magmatic and volcanic phenomena that have been  
1840 modelled in the laboratory and in numerical simulations. In this review we focus on: magma  
1841 chambers (I; see section 5), magma sheet intrusions such as sills and dykes (II, III; see section  
1842 6), lava lakes and lava domes (see section 7), volcanic flows such as lava flows, pyroclastic  
1843 density currents and lahars (IV, V; see section 8), volcanic plumes (VI; see section 9) and  
1844 volcanic ash dispersal (VII; see section 10).

1845



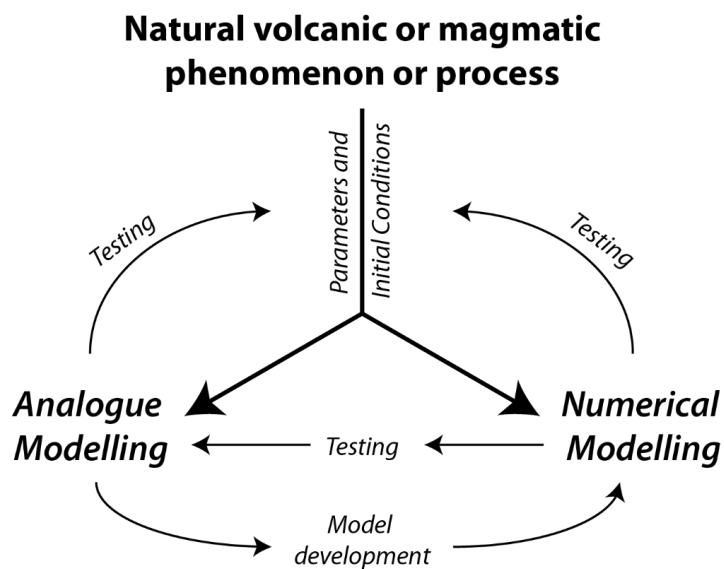
1846

1847 **Figure 2:** Reproduction of Plate IV from Hall (1815). A series of images depict a set of  
1848 experiments which have since inspired the use of analogue materials to provide a physical  
1849 explanation for geological observations made in the field. Hall produced an ‘ideal’ coastal  
1850 section (a) to demonstrate the continuous nature of the folded rock layers observed in the  
1851 field. Sketches depict a set of experiments that were performed (b) by compressing clay layers  
1852 to produce convolutions (c) that are reminiscent of the structures observed in the field.



1853

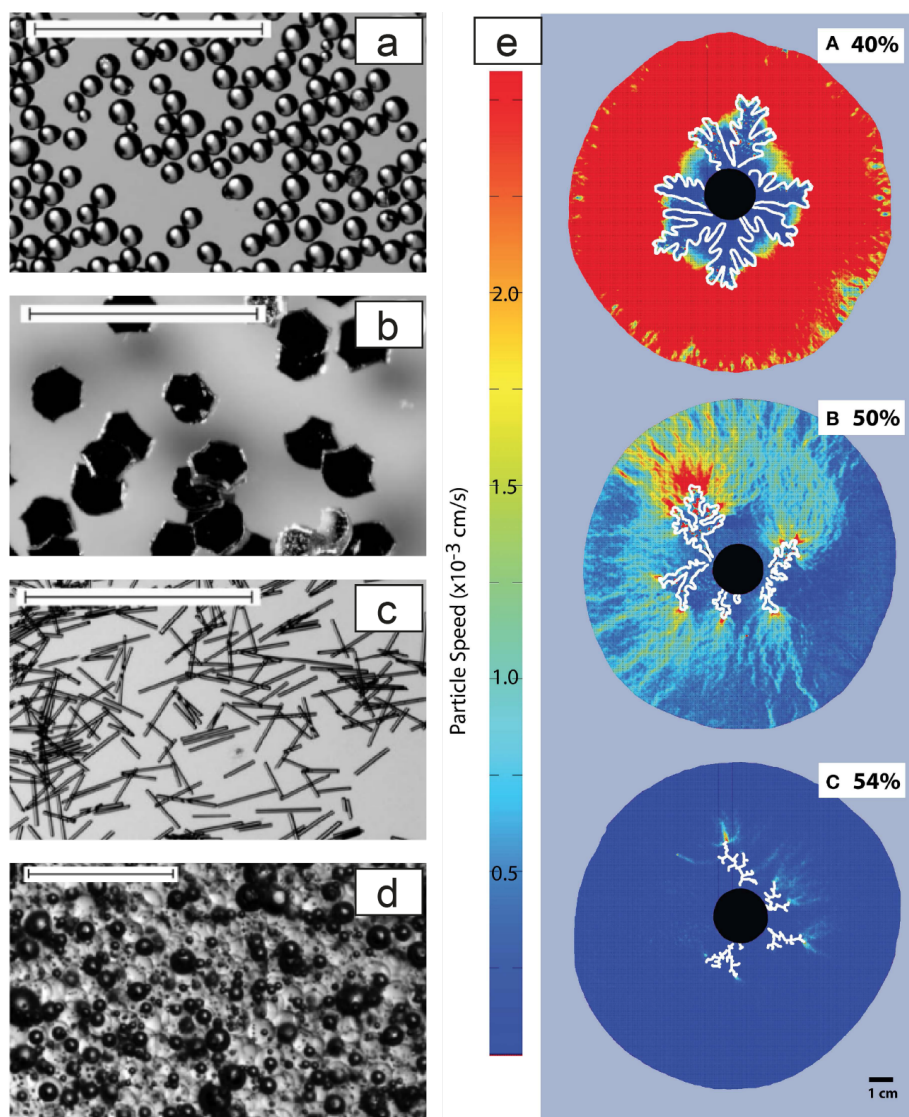
1854 **Figure 3:** Photographs of early analogue experiments that have inspired and informed  
1855 decades of laboratory studies of volcanic and magmatic processes: a) Excavated plaster of  
1856 Paris mixture that was injected into a layered tank of gelatine to model dyke and sill  
1857 emplacement (Hubbert and Willis, 1957), b) water injected into a free-standing triangular  
1858 prism of gelatine to simulate magma intrusion in a volcanic rift (Fiske and Jackson, 1972), and  
1859 c) injection of low density fluid into a uniform ambient fluid (Morton et al. 1956).



1860

1861

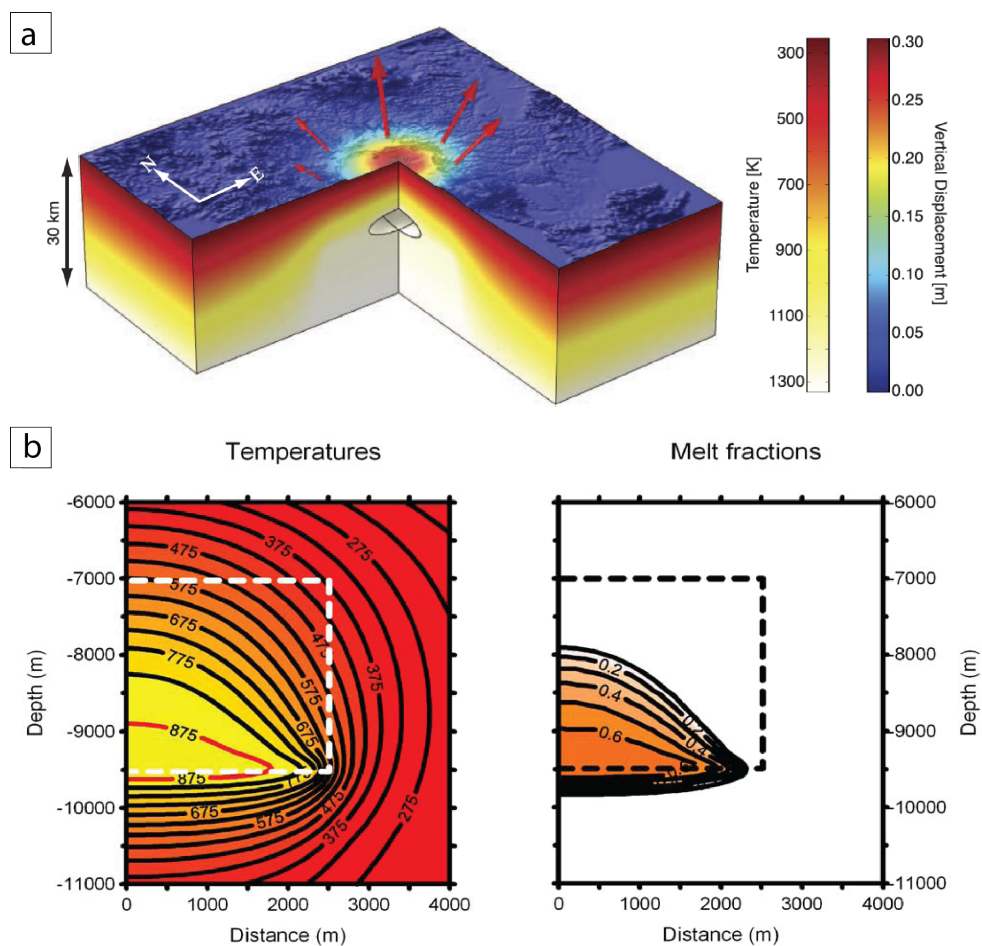
1862 **Figure 4:** A flow diagram to represent the optimal approach to use analogue and numerical  
1863 modelling in volcanology. Observations and measurements from natural volcanic and  
1864 magmatic phenomenon provide the parameters and initial conditions for analogue and  
1865 numerical models; these models are then tested against nature, with analogue models also  
1866 aiding the development of numerical models.



1867

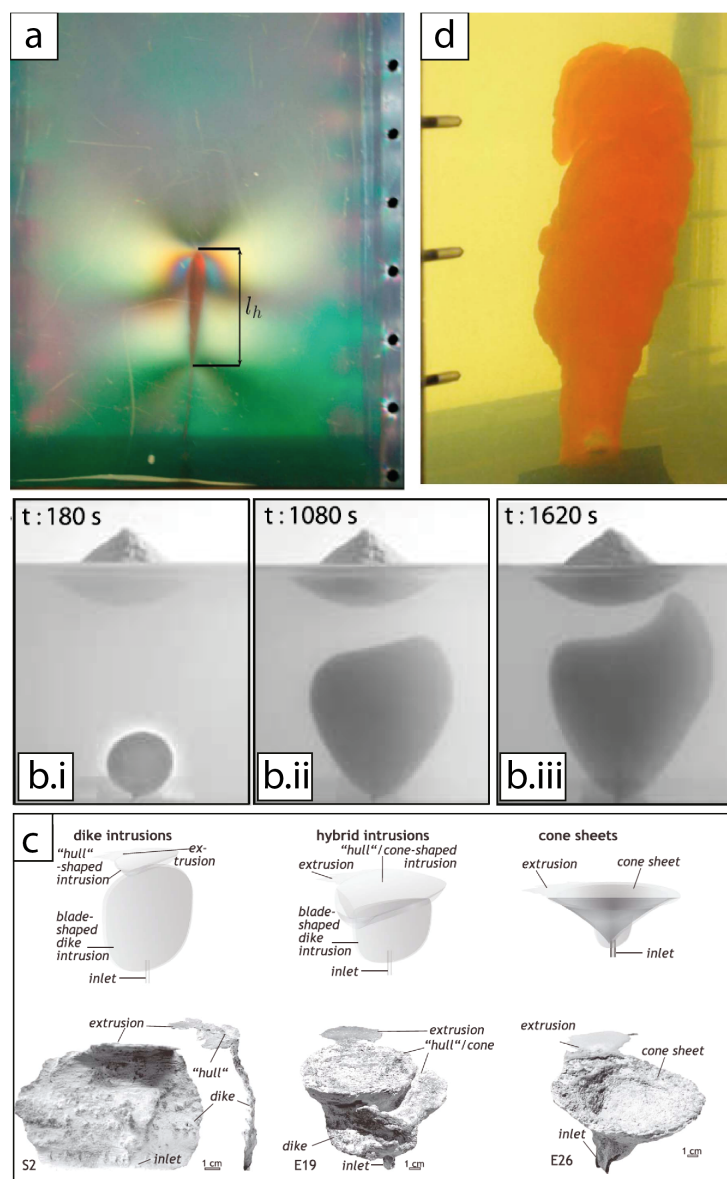
1868

1869 **Figure 5:** Magma rheology studied using analogue materials in laboratory experiments. (a-c)  
1870 spherical glass beads, oblate art glitter, and prolate glass fibres in silicone oil (scale bars 1  
1871 mm; Mueller et al. 2011); (d) three-phase fluid where bubbles (black spheres) and spherical  
1872 glass beads (light translucent particles) are suspended in golden syrup (scale bar 500 µm;  
1873 Truby et al. 2015). (e) Bubble injection experiments using a small-gap parallel plate geometry  
1874 to study the development of permeable pathways in a particle-rich suspension. Particle image  
1875 velocimetry has been used to measure particle speed in three experiments with different  
1876 crystal fraction (Oppenheimer et al. 2015).



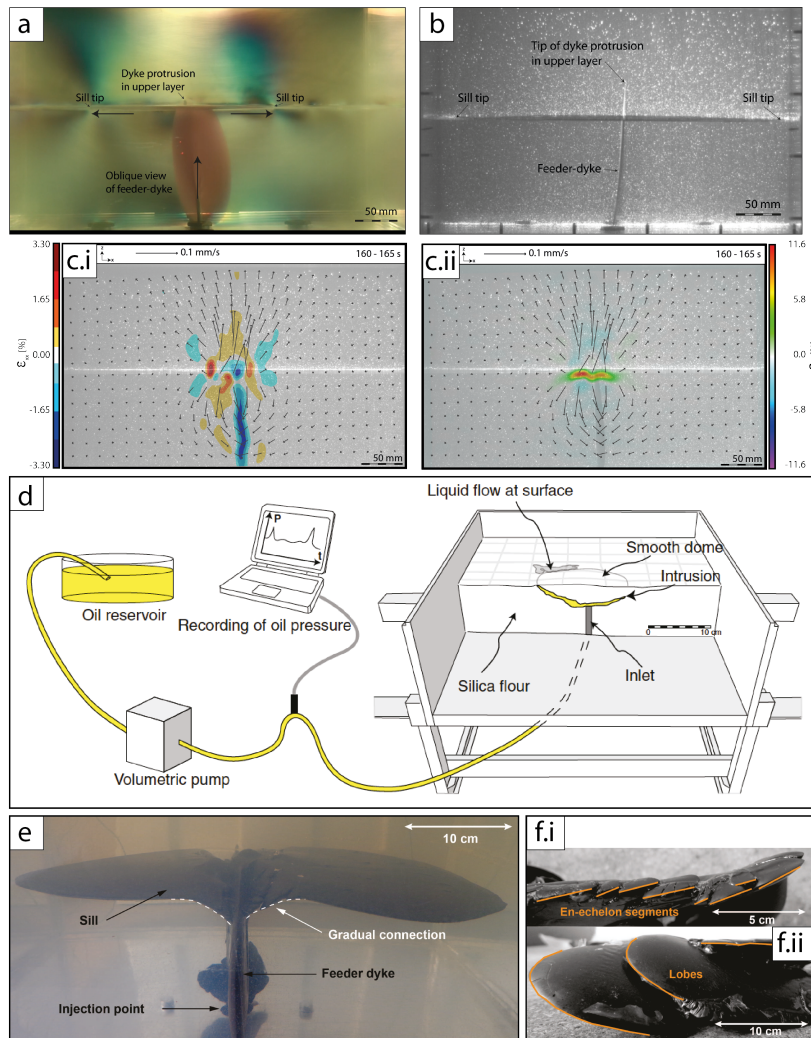
1877

1878 **Figure 6:** Numerical models to simulate magma chamber accretion and associated  
1879 deformation of the crust: a) Thermomechanical model of the magma reservoir at Aira caldera,  
1880 Japan, using a Finite Element model (Comsol Multiphysics) that incorporates the  
1881 temperature-dependent viscoelastic rheology of the crust (Hickey et al. 2016). b) Numerical  
1882 simulation of the magma chamber at Mt Pelee, Martinique, with accumulation of 5 km  
1883 diameter sills at  $15 \times 10^{-4} \text{ km}^3/\text{yr}$  over 62,500 years and solved for the temperature of the  
1884 crust with depth and melt fraction (Annen et al. 2008).



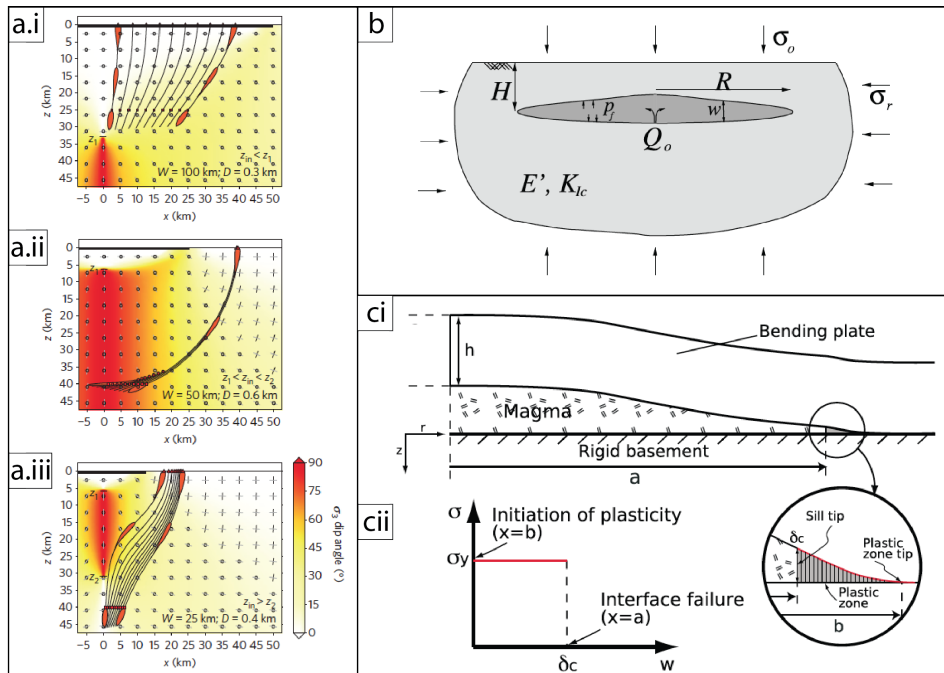
1885

1886 **Figure 7:** A series of photographs demonstrating a range of analogue experiments used to  
 1887 study dyke propagation dynamics. a) Injection of red-dyed isothermal heptane into a gelatine  
 1888 solid, with  $l_h$  indicating the length of the dyke's buoyant head (Taisne and Tait 2011). (b)  
 1889 Series of photographs showing the impact of a volcanic edifice on dyke propagation: injection  
 1890 of dyed water into gelatine with a conical surface load of sand and plaster (Kervyn et al. 2009).  
 1891 c) Schematic sketch and detailed photographs of excavated vegeteline intrusions such as  
 1892 dykes, hybrids and cone sheets formed within compacted silica flour experiments (Galland et  
 1893 al. 2014). d) Injection of a solidifying liquid (wax) causing the formation of an irregular and  
 1894 lobed dyke morphology (Taisne and Tait 2011).



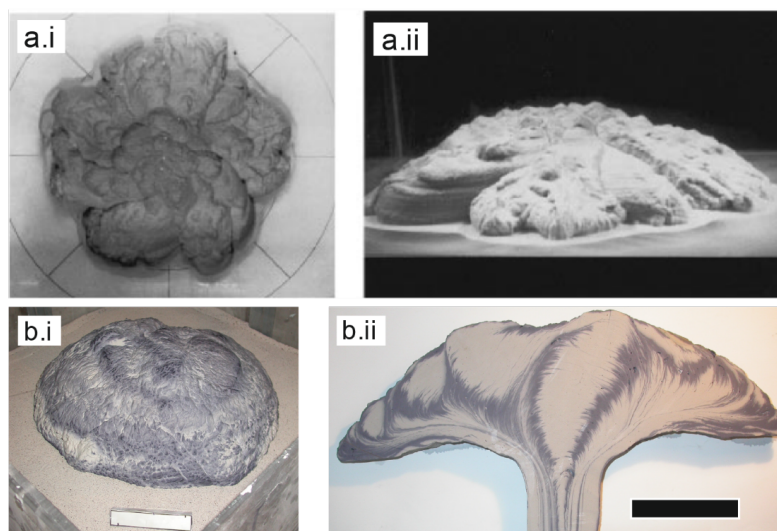
1895

1896 **Figure 8:** Analogue experiments studying sill formation. a-b) Dyke-sill hybrid formation from  
 1897 a feeder dyke in layered gelatine along a weak interface (Kavanagh et al. 2017): a) Polarised  
 1898 light enables stress to be visualised through coloured fringes, and b) a laser-illuminated  
 1899 vertical section through the experiment, showing the sharp boundary between intrusion and  
 1900 host. c) Digital image correlation of sill formation from a feeder dyke in layered gelatine  
 1901 (Kavanagh et al. 2015). Colours indicate incremental strain in the gelatine, and arrows are  
 1902 displacement vectors at the moment of sill formation: i) horizontal incremental strain, and ii)  
 1903 vertical incremental strain. d) Experimental setup where Vegetaline is injected into  
 1904 compacted silica flour to model sheet intrusions (Galland et al. 2014). e-f) Experimental sill  
 1905 formed from a feeder dyke in layered gelatine where solidification effects are considered  
 1906 (Chanceaux 2013): e) Typical sill-forming experiment and f) excavated 3D morphology of  
 1907 Vegetaline sill showing lobed and segmented propagation front (see also Chanceaux and  
 1908 Menand 2014 and 2016).



1909

1910 **Figure 9:** Example numerical models of sheet intrusions: a) dyke trajectories in the presence  
 1911 of a stress barrier (Maccaferri et al. 2014), b) the growth of a laccolith (Bunger and Cruden  
 1912 2011), and c) growth of a laccolith or sill with inelastic deformation (Scheibert et al. 2017).

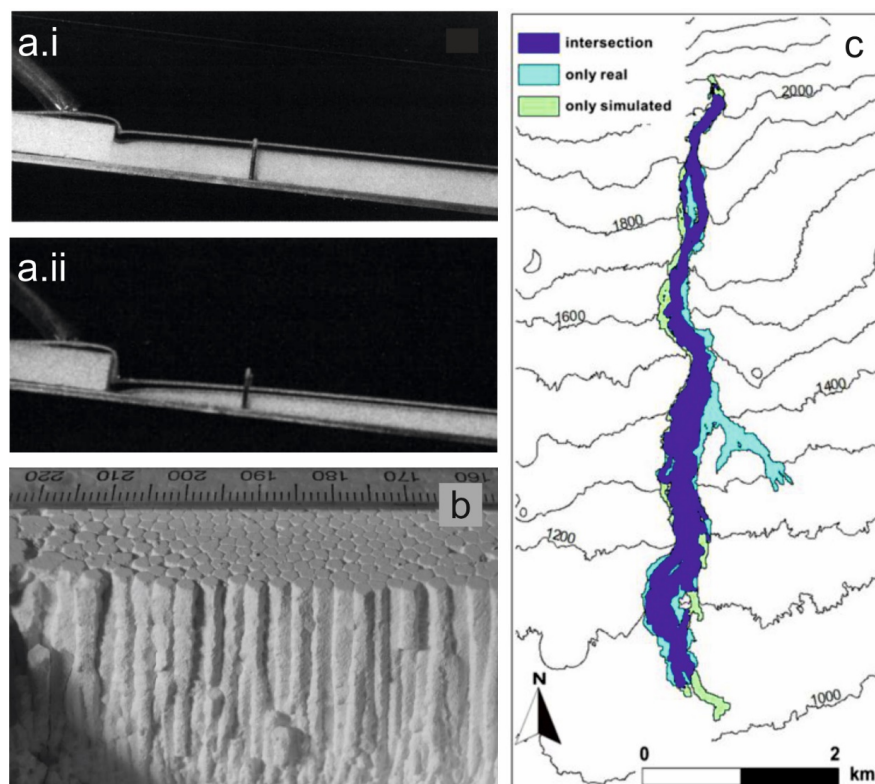


1913

1914 **Figure 10:** Studies of lava dome morphology: (a) Analogue experiment by Griffiths and Fink  
1915 (1997) of polyethylene glycol extruded from a point source imaged in (i) plan view and (ii) side  
1916 view. (b) Photograph showing i) external morphology and ii) cross section through plaster of  
1917 Paris analogue model of lava dome emplacement seeded with magnetic particles for AMS  
1918 (scale bars are 10 cm long, photos courtesy of Prokop Zavada. See also Zavada et al. 2009).

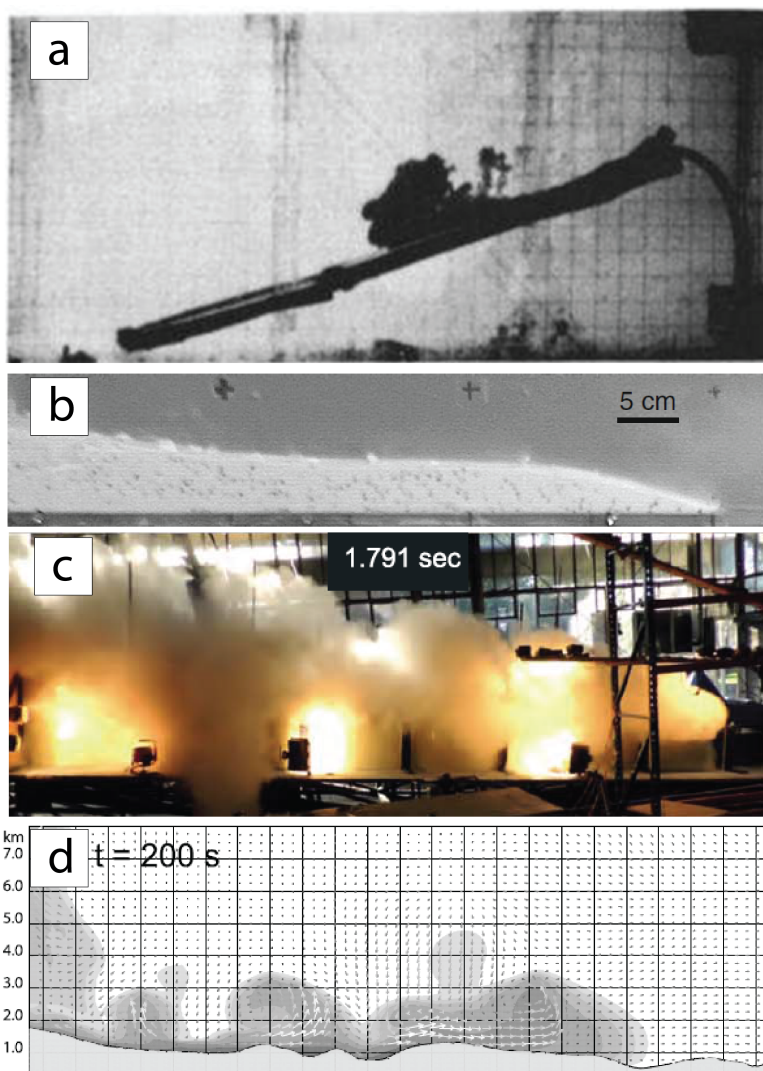


1919



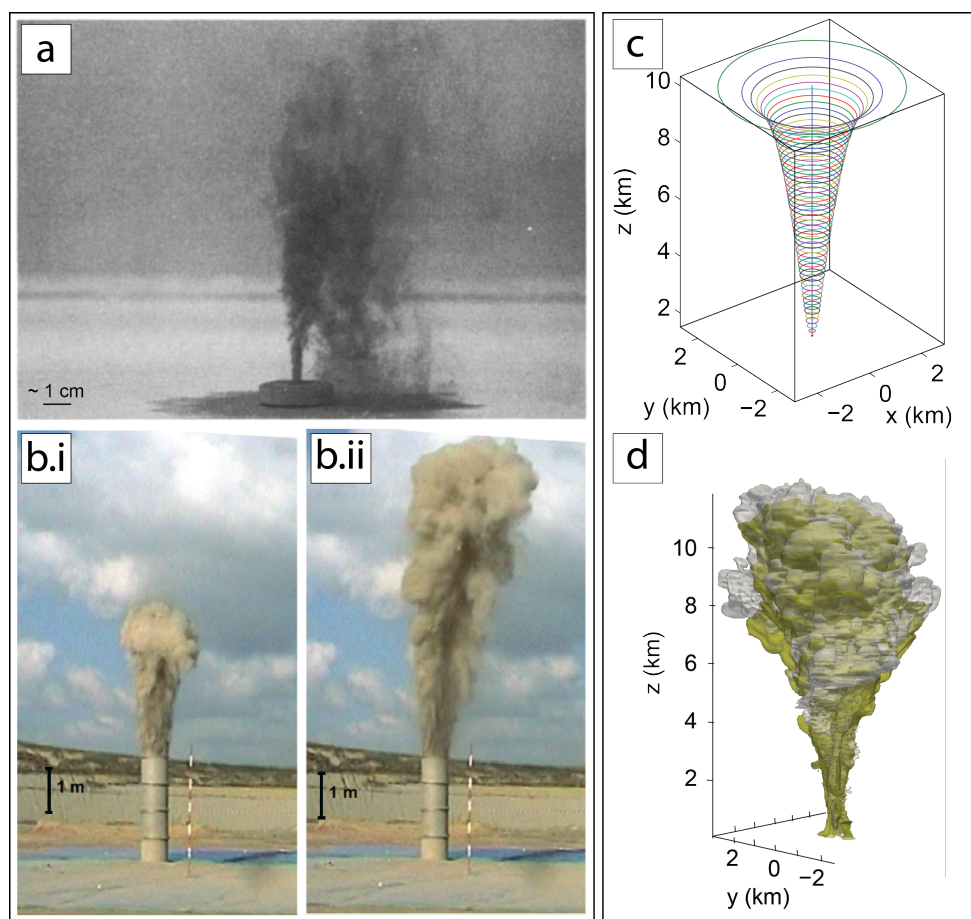
1920

1921 **Figure 11:** Analogue models and numerical simulations of lava flows. a) Effusion of molten  
1922 wax onto bed of solid wax to study thermal erosion of lava flow into underlying material after  
1923 (i) 4 and (ii) 14 minutes (modified from Kerr (2001)). (b) dehydration of corn starch-water  
1924 slurry to study the formation of columnar jointing structures in lava flows (modified from  
1925 Goehring et al. (2006)). c) cellular automata model of lava flow inundation (green and dark  
1926 blue) compared with the flow path of the natural lava flow (light blue and dark blue) effused  
1927 at Mt. Etna, Italy (modified from Rongo et al. (2016)).



1928

1929 **Figure 12:** a) Example of early analogue experiments of particulate flows whereby a mixture  
1930 of methanol, ethylene glycol and water was released on a slope into a tank of fresh water.  
1931 The higher density of the mixture in comparison to the ambient fluid means it flows down  
1932 slope as a gravity current, forming turbulent eddies at the top of the flow (Woods and Bursik  
1933 1994). b) Small-scale experimental model setup designed to investigate particle interactions  
1934 in detail (Roche, 2012). c) Large scale analogue experiments using the PELE setup, allowing  
1935 large scale processes within pyroclastic density currents to be investigated. The figure shows  
1936 emplacement of a dilute mixture of particles and air (Lube et al. 2015). d) Results from  
1937 application of the multiphase numerical model PDAC to the blast phase of the Mount St.  
1938 Helens blast of May 18<sup>th</sup> 1980 (Esposti Ongaro et al. 2012). The models results reproduce  
1939 numerous features of the flows that originated from the blast, including the formation of  
1940 turbulent eddies.



1941

1942 **Figure 13:** Examples of numerical simulations and analogue models of volcanic plumes. a)  
1943 Flume tank analogue experiments of Carey et al (1988) where a particle laden fluid is injected  
1944 into another fluid to investigate plume rise and particle sedimentation dynamics. b) Large  
1945 scale experiments to investigate effects of entrainment coefficient on plume rise (Dellino et  
1946 al. 2014). c) Modelled representation of a vertical plume using the one-dimensional model  
1947 PlumeMoM (Vitturi et al. 2016). d) Three-dimensional model results from the multiphase  
1948 model ASHEE for the same input conditions as c) (Cerminara et al. 2016).